Article

Cell Host & Microbe

Arrhythmic Gut Microbiome Signatures Predict Risk of Type 2 Diabetes

Graphical Abstract

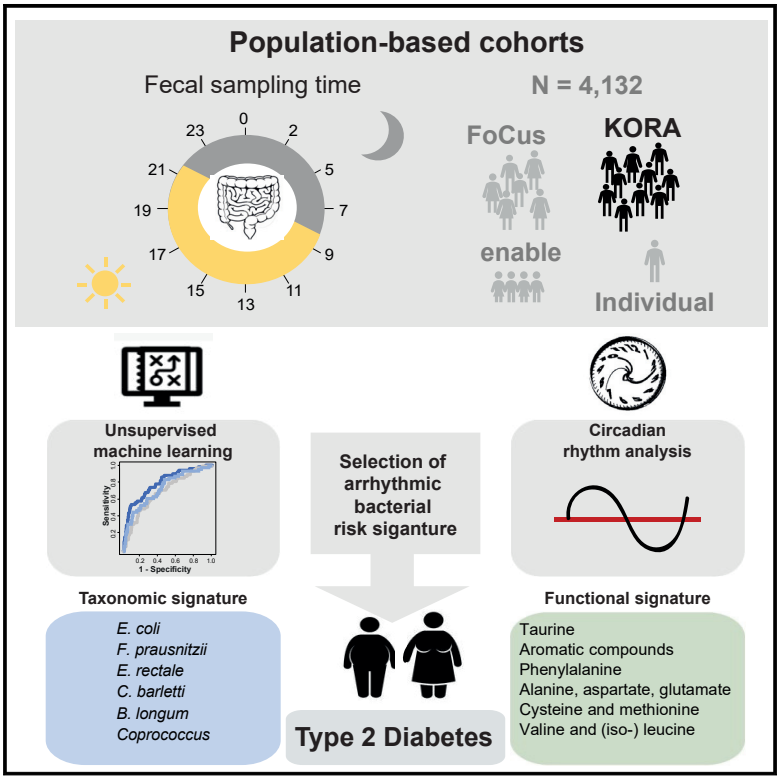

Highlights

- Human gut microbiome exhibits diurnal rhythmicity across populations and individuals
- Obese and T2D individuals show disrupted circadian rhythms in the gut microbiome
- Arrhytmic bacterial signatures contribute to risk classification and prediction of T2D
- These risk signatures show regional differences in applicability across three cohorts

Authors

Sandra Reitmeier, Silke Kiessling, Thomas Clavel, ..., Paul W. O'Toole, Annette Peters, Dirk Haller

Correspondence

dirk.haller@tum.de

In Brief

Reitmeier et al. show that specific gut microbes exhibit rhythmic oscillations in relative abundance and identified taxa with disrupted rhythmicity in individuals with type 2 diabetes (T2D). This arrhythmic signature contributed to the classification and prediction of T2D, suggesting functional links between circadian rhythmicity and the microbiome in metabolic diseases.

Reitmeier et al., 2020, Cell Host & Microbe *28*, 258–272
August 12, 2020
https://doi.org/10.1016/j.chom.2020.06.004

CellPress

CellPress

Cell Host & Microbe

Article

Arrhythmic Gut Microbiome Signatures Predict Risk of Type 2 Diabetes

Sandra Reitmeier,[1,2,14] Silke Kiessling,[1,2,14] Thomas Clavel,[1,3,14] Markus List,[4] Eduardo L. Almeida,[5] Tarini S. Ghosh,[5] Klaus Neuhaus,[1] Harald Grallert,[6] Jakob Linseisen,[6,7] Thomas Skurk,[1] Beate Brandl,[1] Taylor A. Breuninger,[6] Martina Troll,[6] Wolfgang Rathmann,[9] Birgit Linkohr,[6] Hans Hauner,[1,8] Matthias Laudes,[10,11] Andre Franke,[10] Caroline I. Le Roy,[12] Jordana T. Bell,[12] Tim Spector,[12] Jan Baumbach,[4] Paul W. O'Toole,[5] Annette Peters,[6,13] and Dirk Haller[1,2,15,*]

[1]ZIEL - Institute for Food & Health, Technical University of Munich, 85354 Freising, Germany
[2]Chair of Nutrition and Immunology, Technical University of Munich, Gregor-Mendel-Str. 2, 85354 Freising, Germany
[3]Functional Microbiome Research Group, Institute of Medical Microbiology, RWTH University Hospital, Pauwelsstraße 30, 52074 Aachen, Germany
[4]Chair of Experimental Bioinformatics, Technical University of Munich, Maximus-von-Imhof-Forum 3, 85354 Freising, Germany
[5]School of Microbiology and APC Microbiome Ireland, University College Cork, Ireland
[6]Helmholtz Zentrum München and German Diabetes Center (DDZ), Ingolstaedter Landstr. 1, 85764 Oberschleißheim
[7]Chair of Epidemiology, Ludwig-Maximilians University, UNIKA-T Augsburg, Neusässer Str. 47, 86156 Augsburg, Germany
[8]Institute of Nutritional Medicine, Technical University of Munich, Georg-Brauchle-Ring 62, 80992 Munich, Germany
[9]German Diabetes Center (DDZ) and German Center for Diabetes Research (DZD e.V.), Auf'm Hennekamp 65, 40225 Dusseldorf, Germany
[10]Institute of Clinical Molecular Biology, Christian-Albrechts-University of Kiel, Rosalind-Franklin-Straße 12, 24105 Kiel, Germany
[11]Division of Endocrinology, Diabetes and Clinical Nutrition, Department of Medicine, University of Kiel, 24105 Kiel, Germany
[12]Department of Twin Research & Genetic Epidemiology, King's College London, Strand, London WC2R 2LS, UK
[13]Chair of Epidemiology, Ludwig-Maximilians University, Marchioninistr. 15, 81377 Munich, Germany
[14]These authors contributed equally
[15]Lead Contact
*Correspondence: dirk.haller@tum.de
https://doi.org/10.1016/j.chom.2020.06.004

SUMMARY

Lifestyle, obesity, and the gut microbiome are important risk factors for metabolic disorders. We demonstrate in 1,976 subjects of a German population cohort (KORA) that specific microbiota members show 24-h oscillations in their relative abundance and identified 13 taxa with disrupted rhythmicity in type 2 diabetes (T2D). Cross-validated prediction models based on this signature similarly classified T2D. In an independent cohort (FoCus), disruption of microbial oscillation and the model for T2D classification was confirmed in 1,363 subjects. This arrhythmic risk signature was able to predict T2D in 699 KORA subjects 5 years after initial sampling, being most effective in combination with BMI. Shotgun metagenomic analysis functionally linked 26 metabolic pathways to the diurnal oscillation of gut bacteria. Thus, a cohort-specific risk pattern of arrhythmic taxa enables classification and prediction of T2D, suggesting a functional link between circadian rhythms and the microbiome in metabolic diseases.

INTRODUCTION

Increasing evidence links the human gut microbiome to metabolic health (Sonnenburg and Bäckhed, 2016), and altered microbial profiles are associated with obesity, insulin resistance, and type 2 diabetes (T2D) (Goodrich et al., 2014; Karlsson et al., 2013a, 2013b; Pedersen et al., 2016; Qin et al., 2010, 2012; Thingholm et al., 2019; Turnbaugh et al., 2006; Zhou et al., 2019). Population-based studies highlighted a significant degree of variability in inter-individual microbiomes (Falony et al., 2016; Zhernakova et al., 2016), regional effects (He et al., 2018), and drug-associated changes in the gut microbiome (Forslund et al., 2015; Pryor et al., 2019). Despite the extensive efforts to define the role of the gut microbiome in metabolic diseases, especially obesity and T2D, limited reproducibility and specificity of disease-associated taxa across cohorts, e.g., members of *Christensenellaceae*, *Collinsella*, and *Escherichia coli* are also associated with Crohn's disease (Pascal et al., 2017), complicates the identification of microbial risk factors.

The circadian clock, which synchronizes daily food intake behavior and metabolism with the day and night cycle (Panda, 2019), has recently been proposed to influence microbial homeostasis (Thaiss et al., 2014). Daytime-dependent fluctuations were identified in both the oral and fecal microbiota (Kaczmarek et al., 2017; Thaiss et al., 2014). In murine models, circadian rhythms in gut microbiota composition and function are sensitive to diet and feeding patterns (Thaiss et al., 2014;

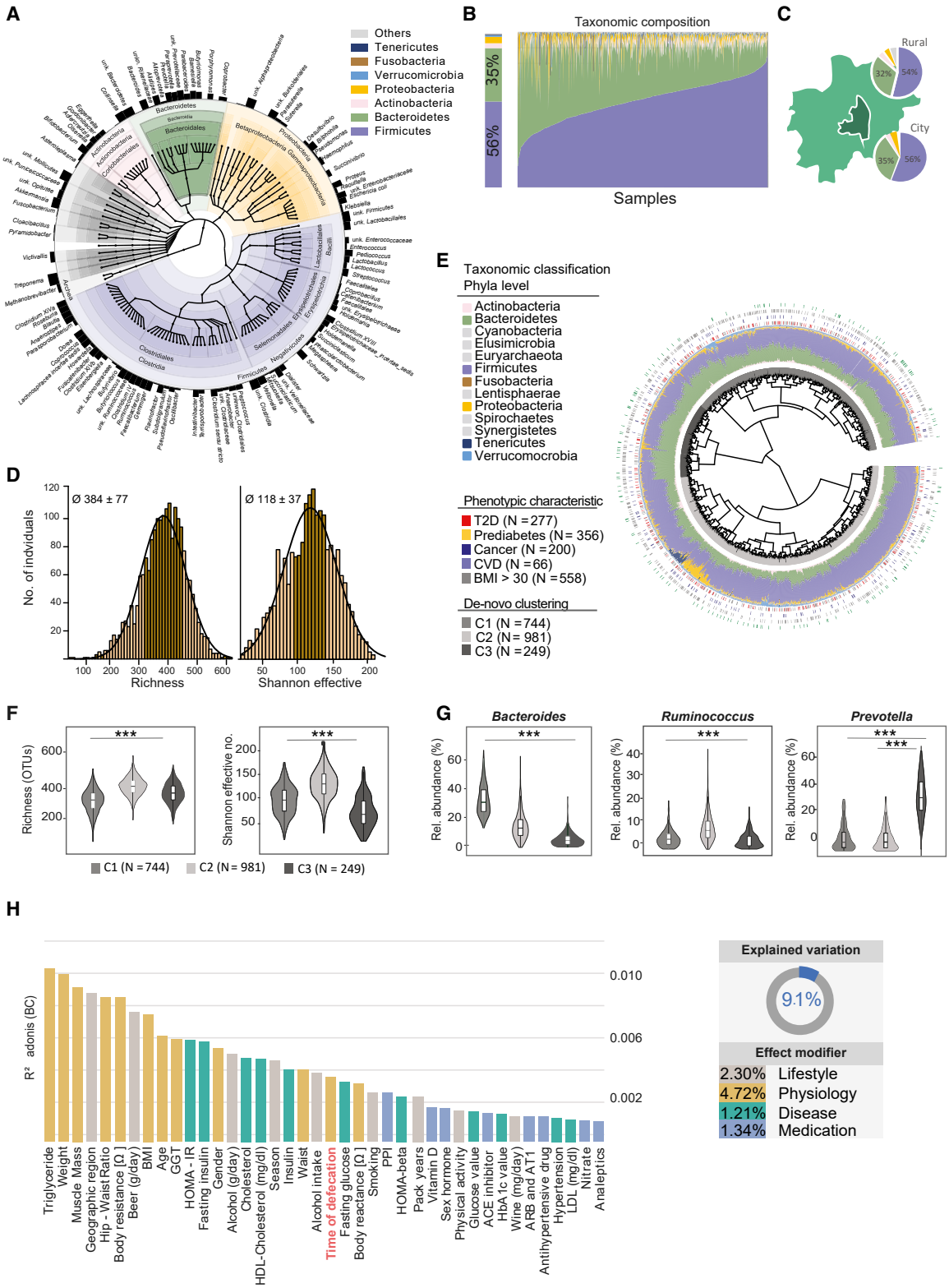

Figure 1. Microbiota Profiling of a Cross-Sectional Population-Based Cohort

(A) Taxonomic tree of the gut microbiota of 1,976 KORA subjects. Colors indicate phyla. Taxonomic ranks are from kingdom (center) to genera indicated by the individual branches. Black bars on the outer ring indicate the prevalence of each genus, the name of which is shown if found in >10% of the individuals (Table S2).

(B) Relative abundances of phyla across the whole cohort. Samples are ordered according to increasing relative abundances of Firmicutes. Colors are as in (A).

(legend continued on next page)

Zarrinpar et al., 2014). Diet-induced obesity dampens cyclic microbial fluctuations in rodents (Leone et al., 2015; Zarrinpar et al., 2014), and epidemiological studies continue to show associations between circadian clock dysfunction due to modern lifestyle and T2D (reviewed in Onaolapo and Onaolapo, 2018), supporting the hypothesis that diurnal oscillations in microbiota composition and function may contribute to metabolic health. The lack of documentation of stool sampling time in addition to the well-documented regional and individual differences in microbiota profiles may account for discrepancies between studies. We therefore suggest to consider circadian oscillations to better understand the underlying mechanisms of disease-associated microbiome alterations and to validate risk profiles in prospective cohorts.

We provide clear demonstration of robust diurnal oscillations in fecal microbiota composition, using stool across a 24-h sampling period of three large-scaled human populations with a total of 4,131 subjects in Germany (KORA, FoCus, and enable). Most importantly, we demonstrate that loss of circadian rhythmicity affects microbiome features related to the onset and progression of T2D and identified bacterial signatures for metabolic risk profiling in human populations.

RESULTS

Microbiota Profiling of the Population-Based Cohort KORA

KORA is a prospective cohort in the region of Augsburg (Germany) designed to understand the role of genetic, lifestyle, and environmental factors in disease progression including metabolic diseases (Table S1). As part of the second follow-up of the S4 KORA cohort, stool was sampled from 1,976 individuals in 2013, for whom we performed high-throughput 16S rRNA gene amplicon sequencing (Tables S2 and S3). Comparing individual microbiota compositions confirmed diverse ecosystems dominated by the two major phyla Firmicutes and Bacteroidetes (cumulative mean relative abundance, 91%) (Figures 1A and 1B). In comparison with other studies, compositional variations were marginally affected by geography (0.9%), since KORA is restricted to a single city (Augsburg, Bavaria, Germany) and its close surrounding (Arumugam et al., 2011; He et al., 2018; Yatsunenko et al., 2012) (Figure 1C). The cohort was characterized by an average individual richness of 348 ± 77 operational taxonomic units (OTUs) and 118 ± 37 Shannon effective number of species (Figure 1D).

Unsupervised analysis based on generalized UniFrac distances identified three fecal microbiota clusters (C1, N = 744; C2, N = 981; C3, N = 249) similar to previously reported enterotypes (Arumugam et al., 2011) (Figures 1E, 1F, and S1A). Individuals in C1 had the lowest microbiota richness and showed significantly higher relative abundances of *Bacteroides*. The most diverse cluster C2 (highest number of subjects) was dominated by members of the genus *Ruminococcus*, while *Prevotella* dominated in C3 (Figure 1G). Individuals with obesity (BMI $\geq$ 30, N = 558), T2D (N = 277), and prediabetic conditions (N = 356) classified according to their oral glucose tolerance (WHO criteria), cancer (N = 200) as well as cardiovascular disease (CVD) (N = 66) were evenly distributed across these clusters (Figure 1E). Multivariate analysis of metadata co-varying with the fecal microbiota profiles identified 40 of 113 features related to physiology (e.g., blood triglyceride levels, body weight, muscle mass, and time of defecation), lifestyle and environment (geographical region, beer/alcohol consumption, and seasons), disease-associated parameters (mostly related to glucose metabolism), and medication, collectively explaining 9.1% of variability (Figure 1H).

Diurnal Rhythms in Fecal Microbiota Composition

Time of defecation was among the most significant factors (p value = 0.004; R^2 = 0.001) explaining inter-individual variabilities in microbiota structure (Figure 1H). Thus, diurnal rhythmicity of fecal microbiota profiles was studied in 1,943 subjects for whom time at sampling was available (Figures 2A–2C). Community diversity (both species richness and Shannon effective number of species) fluctuated significantly throughout the day (Figure 2A). Diurnal rhythmicity was also evident in relative abundances of the two most dominant phyla, which oscillated in antiphase. Bacteroidetes showed 6% higher mean relative abundance at night, whereas the phylum Firmicutes was higher during the day. Since more than 70% of all samples were collected at morning hours between 5 and 11 am, we re-analyzed the data using 10 random sub-samples of 25 patients for every time point and thereby confirmed initial results including all subjects (Figure S1A).

After removal of OTUs low in mean relative abundance (<0.1%) and prevalence (<10% subjects), the heatmap of remaining 422 OTUs illustrated heterogeneous distribution of their peak relative abundances, ranging from early day to late night, suggesting that the microbiota at different times of the day are dominated by different microbial taxa (Figure 2B; Table S7). According to cosine-wave regression analysis, 15.2% of the OTUs

(C) Geographical map of the city of Augsburg (Bavaria, Germany) and its rural area. Subjects are grouped according to their place of residence. The pie charts show taxonomic distributions at the phylum level (colors as in A) in individuals living outside (rural) or in the city (city).

(D) *Alpha*-diversity of the fecal microbiota in KORA. Richness (left; 384 ± 77) and Shannon effective number of species (right; 118 ± 37), which were both not normally distributed across the whole cohort (Shapiro test > 0.05).

(E) *Beta*-diversity of the fecal microbiota in KORA. The dendrogram shows similarities between microbiota profiles based on generalized UniFrac distances between 1,976 subjects represented by individual branches. Unsupervised hierarchical clustering identified three main clusters of individuals (gray scale next to branches). Individual taxonomic composition at the phylum level is shown as stacked bar plots around the dendrogram (colors as in A). Bars in the outer part of the figure indicate disease status: first ring, diabetes (red, T2D; gray, prediabetes; no color, nonT2D); second ring, cancer (blue); third ring, obesity (gray, BMI $\geq$ 30); fourth ring, cardiovascular diseases (green).

(F) Differences in *alpha*-diversity between the *de-novo* clusters from E (colors also follow E).

(G) Differences in relative abundances of the three genera *Bacteroides*, *Ruminococcus*, and *Prevotella* for the three microbiota clusters as in Figure 1E. ***p $\leq 1 \times 10^{-5}$.

(H) Explained variations in fecal microbiota composition by covariates. All variables shown had a significant influence (p $\leq$ 0.05), displayed as proportions of explained variations based on R^2 calculated by multivariate analysis of Bray-Curtis dissimilarity.

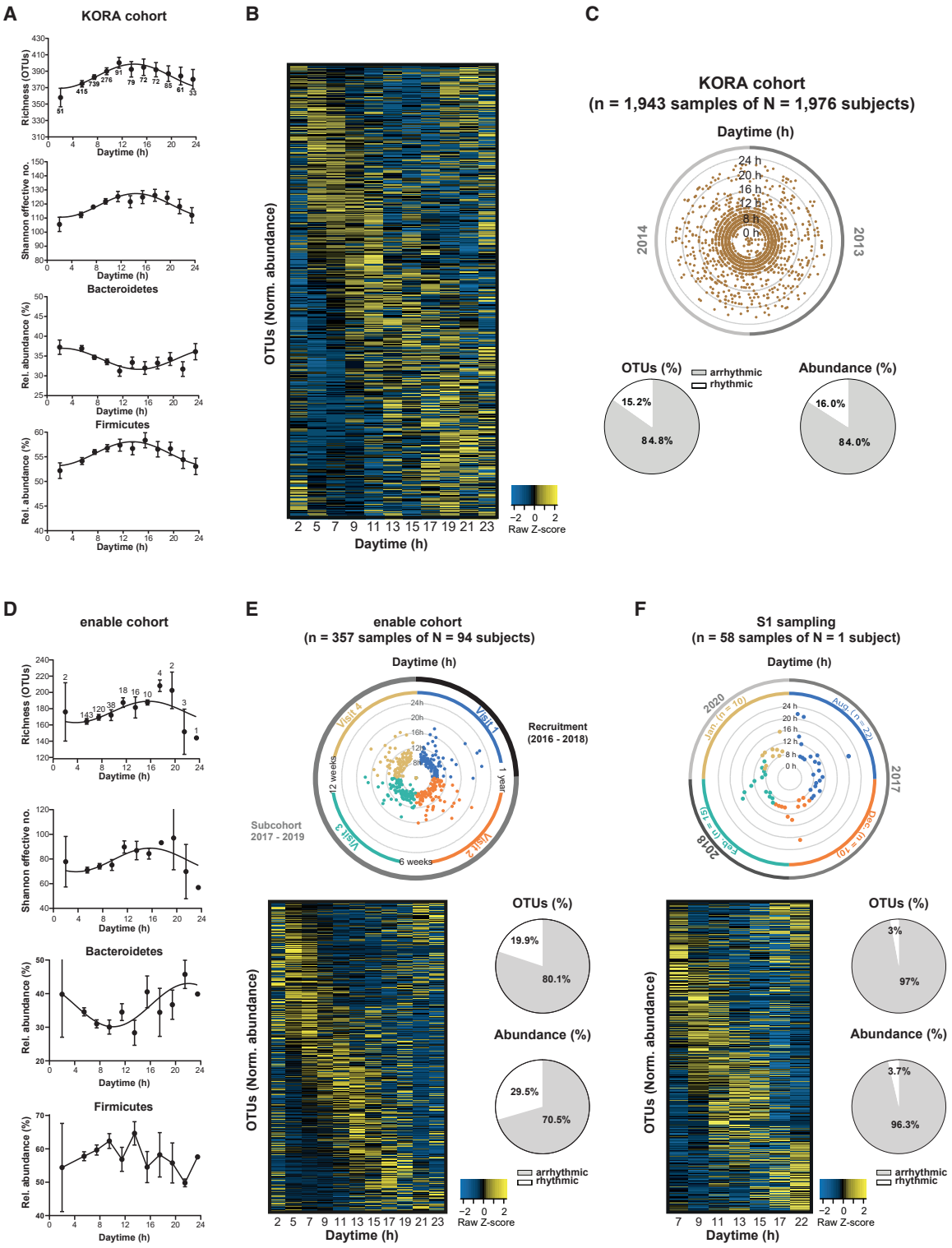

Figure 2. Diurnal Rhythms in the Human Gut Microbiota

(A) Diurnal profiles of *alpha*-diversity and of relative abundances of the phyla Bacteroidetes and Firmicutes in 1,943 subjects with known defecation time. Significant rhythms are illustrated with fitted cosine-wave curves (cosine-wave regression, $p \leq 0.05$). Data are represented as mean ± SEM.

(B) Heatmap depicting the overall phase relationship and periodicity of 422 OTUs (mean relative abundance > 0.1%; prevalence > 10% individuals) ordered by their cosine-wave peak phase according to time of day and normalized to the peak of each OTU.

(C) Amount of rhythmic (white) and arrhythmic (gray) OTUs and their relative abundance in percent (compare with B).

(legend continued on next page)

were rhythmic (rOTUs) (Figure 2C). Similar proportions of rOTUs were identified using other non-parametric (12.3%) and parametric methods (13.5%; Figure S1B), demonstrating validity of the analysis. Oscillating fluctuations in alpha-diversity and Bacteroidetes as well as similar numbers of significant rhythmic OTUs were confirmed in a smaller, age-matched, and regionally nearby located (Munich/Freising), independent cohort with multiple sampling per person (enable cohort N = 93 subjects with n = 357 fecal samples, 19.9% rOTUs, Figures 2D and 2E). Even in a single individual (subject 1, S1), for whom 58 samples were collected consecutively over 3 years, microbiota oscillations (3% rOTUs) were demonstrated (Figure 2F).

Microbial Oscillations Are Disrupted in Obesity and T2D

Since KORA is best suited for the study of metabolic conditions, we focused on obese, prediabetic, and T2D subjects. Species richness and *alpha*-diversity were lower in individuals with T2D and obesity (BMI $\geq$ 30), whereas Firmicutes-to-Bacteroidetes ratios remained unchanged compared with healthy subjects (Figure 3A). Significantly different relative abundances were identified for 30 OTUs in T2D subjects (N = 277) versus all others (N = 1,270) (Figure 3B; Table S7). Robust daily oscillations in *alpha*-diversity, phyla, and molecular species were observed in KORA subjects without T2D (nonT2D, N = 1,255) and subjects with BMI < 30 (N = 1,393) (Figures 3C–3E, S1C, and S1D). In contrast, rhythmicity in *alpha*-diversity and phylum proportions (Bacteroidetes and Firmicutes) were absent in subjects with either T2D (N = 401) or a BMI $\geq$ 30 (N = 545) (Figures 3C–3E). A heatmap showing peak relative abundances of OTUs confirmed the disruption of rhythmicity in subjects with T2D regardless of BMI (Figure S1D). All 10.4% OTUs that oscillated in nonT2D subjects lost rhythmicity in subjects with T2D (Figure S1C). Of note, 3.5% of OTUs gained rhythmicity in T2D cases (Figure S1C). To account for the difference in sample size between subject groups (T2D, N = 269; nonT2D, N = 1,255), the circadian analysis was validated using 10 different randomly selected and sample size-matched groups (Figure S1E). Loss of diurnal oscillations in diabetic subjects was well reflected in the relative abundances of single OTUs (Figures 3D and S1C). OTUs with disrupted rhythmicity in T2D were largely (>60%) not shared with arrhythmic OTUs in obese individuals, indicating a BMI-independent loss of rhythmicity in T2D (Figure 3F). Interestingly, intermediate phenotypes were noted in prediabetic subjects (N = 352) with a loss of rhythmicity for the two major phyla but not *alpha*-diversity (Figure 3C). In prediabetes, the proportion of rOTUs was reduced from 10.4% to 7.6% (Figures 3D and S1C). Similar results were obtained using JTK_CYCLE or harmonic cosine-wave regression, demonstrating robustness of the findings (Figure S1C).

We identified 87 OTUs that oscillated in controls but lacked rhythmicity in T2D. They belonged to the genera *Akkermansia*, *Bacteroides*, *Bifidobacterium*, *Blautia*, *Clostridium*, *Coprococcus*, *Dorea*, *Prevotella*, *Roseburia*, and *Ruminococcus* (Figure 3G; Tables S2 and S7), which accords with recently published data describing oscillations in two subjects (Thaiss et al., 2014). Interestingly, the majority of these arrhythmic OTUs (66 from 87) identified in T2D also lost rhythmicity in prediabetes. In addition, the comparison of two paired stool sampling times with more than 8-h distance in the prospective subcohort of KORA confirmed the presence of daytime-related differences in nonT2D and, most importantly, also confirmed their absence in T2D (Figure S3B), supporting at least to some extent the population data at individual levels. Altogether, these population-based findings clearly indicate that rhythmicity of the fecal microbiota is disrupted in subjects with obesity and T2D.

Analysis of eating behavior and dietary intake as influencing factors for time related microbial shifts (Collado et al., 2018) showed no significant differences between nonT2D, prediabetes, and T2D subjects. The number of meals individuals were consuming over one day was equally distributed among the groups with a similar total caloric intake for the groups. No difference was found in the type of consumed meals, e.g., no preferences of late-night eating within one group (Figure 4A), suggesting that eating habits and dietary intake are most likely not the underlying reasons to explain arrhythmicity of microbiota composition observed in T2D cases. Of note, percentage of missing or incomplete information varied between the groups: 7.1% of nonT2D and 20.2% of subjects with T2D provided no or insufficient dietary information. This highlights the problems of dietary assessment, including validity and misreporting (King et al., 2016) and argues for the combination of food questionnaires with objective biomarkers (Figure 4B).

Classification of T2D Using Arrhythmic Microbial Signatures

We then sought to identify diagnostic biomarkers for T2D development using microbiota profiles of 1,340 subjects sampled in 2013 as training data and another 699 subjects for whom matched samples at the 5-year follow-up (2018) were available as independent test data (Figure 5A; Table S3). Among the 87 arrhythmic OTUs (Figure 3G), we selected 13 arrhythmic OTUs (s-arOTUs) with differential 24-h time-of-day patterns using the detection of differential rhythmicity (DODR) R packages (Thaben and Westermark, 2016) (Figure 5B; Table S7), which overlap with the 30 differentially abundant OTUs detected in the whole cohort (Figure 3B). We trained a generalized linear model (GLM) on these 13 s-arOTUs to classify T2D. The model performed significantly better than an equal number of randomly selected control

(D) Diurnal profiles of *alpha*-diversity and of relative abundances of the phyla Bacteroidetes and Firmicutes in 94 subjects (with multiple time points) with known defecation time. Significant rhythms are illustrated with fitted cosine-wave curves (cosine-wave regression, $p \leq 0.05$). Data are represented as mean ± SEM.
(E) Upper part: scheme showing the sampling time points and their distances for the enable cohort. Lower part: heatmap depicting the overall phase relationship and periodicity of OTUs in the enable cohort (N = 388 OTUs from n = 372 samples and N = 94 subjects; mean relative abundance >0.1%; prevalence >10% individuals) ordered by their cosine-wave peak phase according to time of day and normalized to the peak of each OTU. Amount of rhythmic (white) and arrhythmic (gray) OTUs and their relative abundance in percent.
(F) Upper part: scheme showing the sampling time points and their distances for the single male individual S1. Lower part: heatmap depicting the overall phase relationship and periodicity of OTUs in one subject (N = 384 OTUs from 58 longitudinal samples; mean relative abundance >0.1%; prevalence >10% individuals) ordered by their cosine-wave peak phase according to time of day and normalized to the peak of each OTU. Amount of rhythmic (white) and arrhythmic (gray) OTUs and their relative abundance in percent.

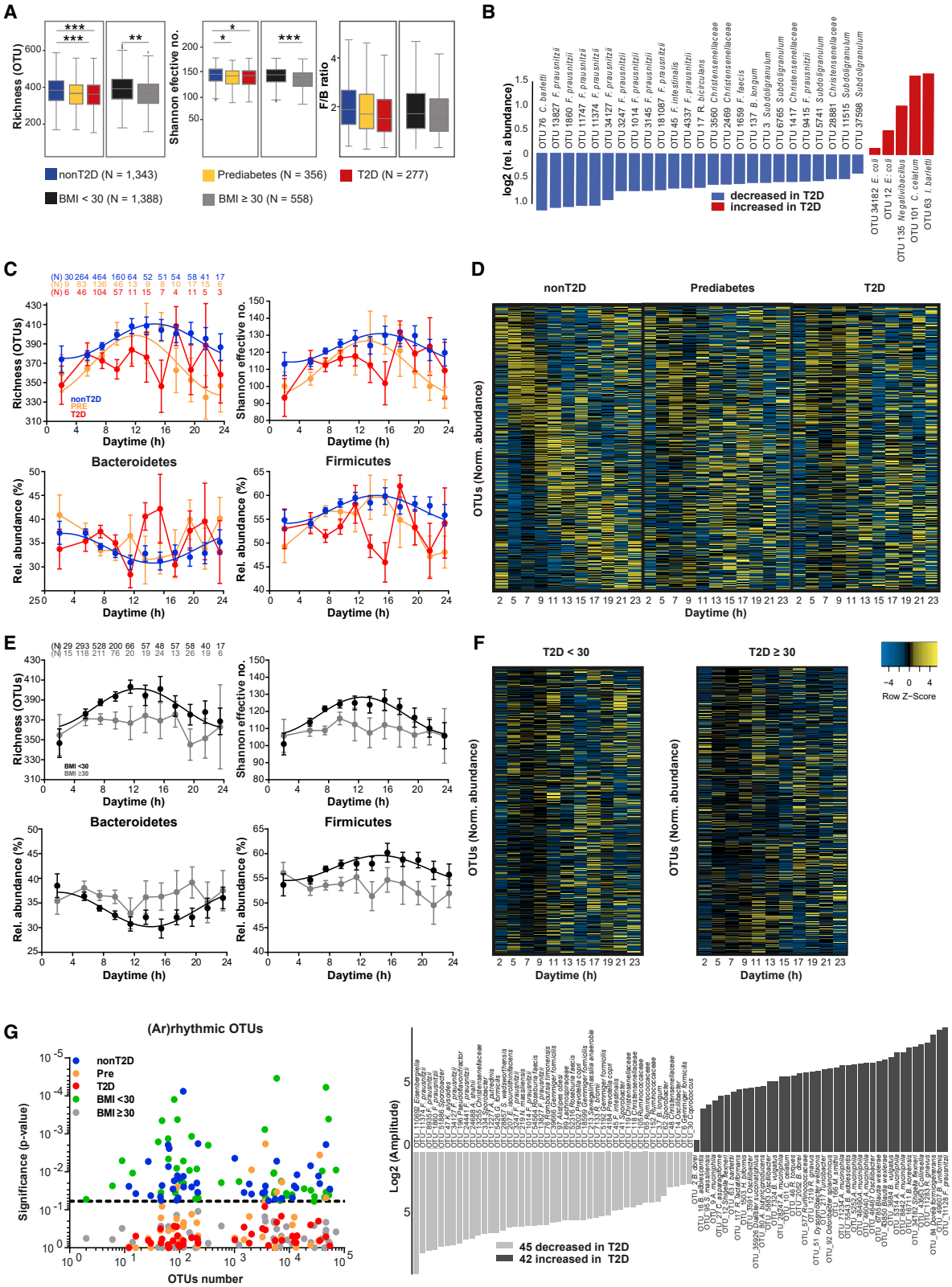

Figure 3. Disrupted Microbial Oscillation in Obesity and T2D

(A) Significant differences in richness (nonT2D = 391 ± 75; prediabetes = 372 ± 76; T2D = 371 ± 79; p value = 0.0002 and BMI < 30 = 390 ± 76; BMI ≥ 30 = 368 ± 76; p value < 10^{-8}) and shannon effective number (nonT2D = 121 ± 37; prediabetes = 112 ± 36; T2D = 114 ± 37; p value = 0.0037 and BMI ≥ 30 = 121 ± 37; BMI

(legend continued on next page)

OTUs (rndOTUs), which were not rhythmic in either of the groups (repeated 100 times, mean area under curve [AUC] = 0.79 versus 0.59; p value for 100 permutations = 2.03×10^{-8}) (Figure 5C). As a complementary and hypothesis-free approach for identifying T2D biomarkers, we also trained a random forest (RF) model, in which a 5-fold cross validation was applied to 80% of the data, while the remaining 20% were used to assess performance. We repeated this random split 100 times and identified 63 out of 425 OTUs that were consistently selected as being predictive, with a mean AUC of 0.73 on the test set (Figure 5D). BMI, as an additional variable in the model, reduced the number of selected OTUs to 14 (rfOTUs) with significant differences in relative abundance (mean AUC = 0.77, Figures S2I and 3B; Table S7). This signature included *Bifidobacterium longum* (OTU 37), *Clostridium celatum* (OTU 101), *Intestinibacter bartlettii* (OTU 63), *Romboutsia ilealis* (OTU 76), and several taxa closely related to *Fecalibacterium prausnitzii* (OTU 1,014, OTU 1,860, OTU 3,247, OTU 11,374, and OTU 34,127) and *Escherichia coli* (OTU 12 and OTU 34,182). However, a model trained on the outcome obesity was not able to differentiate T2D (mean AUC = 0.68), suggesting that the selected 14 rfOTUs are not merely surrogates of the confounding variable BMI (Figure S2B). In reverse, the selected 14 rfOTUs failed to differentiate obesity (mean AUC = 0.63; Figure S2B), supporting the finding that obesity and T2D differentially affect microbiota profiles. In addition, BMI did not perform well in a mixed effect RF model (AUC = 0.69; 63 selected OTUs; Figures S4F and S4G). Strikingly, 13 of these 14 rfOTUs are the same as the above identified 13 s-arOTUs (Figures 5B and S2I), supporting the importance of arrhythmic OTUs in the diabetic risk signature. We further show robustness of our results when adjusting for compositionality bias (Tsilimigras and Fodor, 2016) (Figure S4E). A GLM using the selected rfOTUs and BMI (rfOTUs + BMI) classified T2D with an AUC of 0.79, performing significantly better than a set of 14 randomly picked OTUs (rndOTUs, AUC = 0.60; repeated 100 times, Figure 5E). Due to a comparable performance of both models and the extensive overlap of OTUs, all 13 s-arOTUs were used for further analysis. The integration of miscellaneous diabetes risk markers improved the classification up to an AUC of 0.87. A RF model trained on an expanded set of miscellaneous risk markers selected 9 OTUs which are all shared with the 13 s-arOTUs (Figure S2C).

In agreement with previous results (Forslund et al., 2015; Pryor et al., 2019), metformin (MET) intake significantly affected T2D classification (+MET T2D AUC = 0.87 versus −MET T2D AUC = 0.60; Figure S2D), but a risk signature based on +/MET intake was not able to classify T2D in the KORA cohort (AUC = 0.60; Figure S2E). Although MET was found to synchronize peripheral circadian clocks (Barnea et al., 2012), indicating that MET may directly interfere with the circadian analysis, MET did not change rhythmicity in *alpha*-diversity and phyla nor the overall percentage of rOTUs in subjects with T2D in our study (Figures S2F and S2G). Of note, 9 of 14 OTUs that gained rhythmicity in T2D showed diurnal oscillation in T2D only when taking MET and, thus, may represent rather protective OTUs. Importantly, none of the rOTUs identified in +/−MET-T2D overlap with the 13 s-arOTUs used for the classification of T2D (Figure S2H). Consequently, MET did not affect the predictability of T2D based on the s-arOTU signature. Considering the fact that 5 OTUs gained rhythmicity in T2D, these OTUs may have been chosen alternatively for T2D classification, nevertheless we focused on the larger proportion of arrhythmic OTUs.

Validation of Arrhythmic Microbial Signatures in Independent and Prospective Cohorts

Disruption of microbial rhythmicity in T2D was confirmed in another large-scaled and KORA-independent cohort from the northern part (Kiel) of Germany (FoCus: N = 1,070 nonT2D, N = 293 T2D) (Relling et al., 2018). Loss of daily oscillations in richness and *alpha*-diversity was associated with a significant reduction of rhythmic OTUs in T2D (1.4% rOTUs) compared with nonT2D (8.5% rOTUs) (Figure 5F). Based on a BLAST search we assigned the corresponding s-arOTU and presented the differences in relative abundances between nonT2D and T2D (Figure S2J; Table S8). In combination with BMI the relative abundance values were considered as input for the imported KORA GLM, classifying T2D with an AUC of 0.76 and respective values for sensitivity and specificity of 75% and 69% (Figures 5G and 5H). Interestingly and different from FoCus, the across country validation of the T2D risk signature using the twin cohort from

≥ 30 = 110 ± 37; p value < 10^{-10}) and Firmicutes-to-Bacteroidetes ratios depending on metabolic status nonT2D = 2.08 ± 1.30; prediabetes = 2.03 ± 1.34; T2D = 1.80 ± 1.16; p value = 0.58 and BMI < 30 = 2.1 ± 1.31; BMI ≥ 30 = 1.82 ± 1.19; p value = 0.73) (red, T2D; yellow, prediabetes; blue, nonT2D; gray, BMI ≥ 30; black, BMI < 30).

(B) Thirty OTUs with significantly different relative abundances between T2D and nonT2D subjects (Table S6). Species names are given to the closest match in a BLASTn search.

(C) Diurnal profiles of *alpha*-diversity and of relative abundances of the phyla Bacteroidetes and Firmicutes of subjects with diabetes (T2D, red; N = 269), with prediabetes (Pre, orange; N = 352), or without diabetes (nonT2D, blue; N = 1,254). Significant rhythms (cosine-wave regression, p ≤ 0.05) are illustrated with fitted cosine-wave curves; data points connected by straight lines indicate no significant cosine fit curves (p > 0.05) and thus no rhythmicity. Data are represented as mean ± SEM.

(D) Heatmaps of the normalized daytime-dependent relative abundance of OTUs based on 422 OTUs (see A). Data are normalized to the peak of each OTU and ordered by the peak phase according of subjects without diabetes (left, nonT2D), with prediabetes (middle), or with diabetes (right, T2D).

(E) As (A), of subjects with diabetes (T2D), either shown for a BMI < 30 (black, N = 1,393) or a BMI ≥ 30 (gray, N = 545) Significant rhythms (cosine-wave regression, p ≤ 0.05) are illustrated with fitted cosine-wave curves; data points connected by straight lines indicate no significant cosine fit curves (p > 0.05) and thus no rhythmicity. Data are represented as mean ± SEM.

(F) As (B), but of subjects with diabetes (T2D) and a BMI < 30 (left, N = 124) or a BMI ≥ 30 (right, N = 145).

(G) Quantification of rhythmicity from OTUs in B shows diurnal rhythms in control groups (nonT2D, dark green, N = 1,254; BMI < 30, light green, N = 546), which are arrhythmic in disease stages like prediabetes (Pre, orange, N = 352), diabetes (T2D, red, N = 269), or obesity (BMI ≥ 30, gray, N = 1,396). Significance of rhythmicity (y axis) is indicated by p values above the dashed line (p ≤ 0.05; cosine-wave regression). Right panel: amplitude of the cosine curve of OTUs that are rhythmic in healthy controls but arrhythmic in T2D. Of 422 OTUs (see Figure 1I), 87 OTUs oscillated in controls only. These OTUs are ordered according to their fluctuation amplitude in healthy controls: light gray, decreased; dark gray, increased in relative abundance in T2D compared with nonT2D (Table S7).

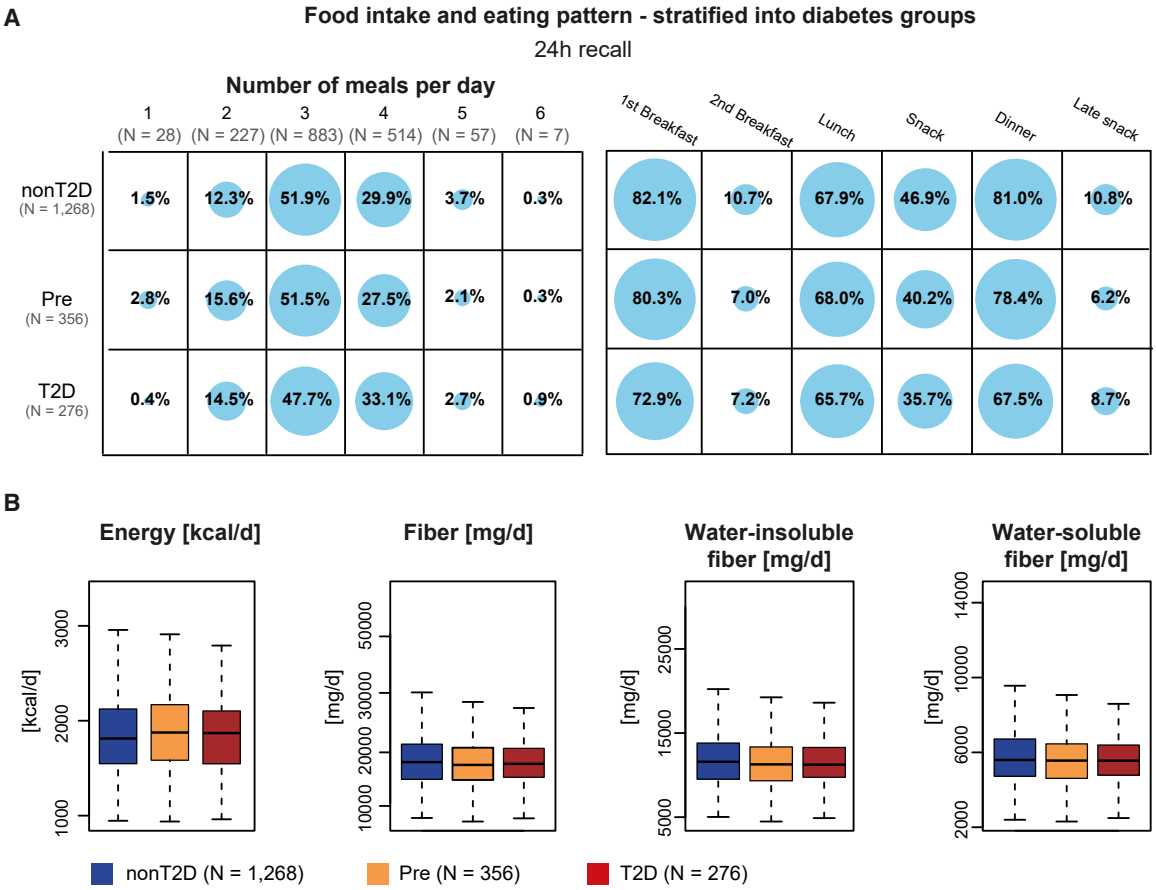

Figure 4. Dietary Habits and Food Intake between NonT2D, Prediabetes, and T2D

(A) Meal frequencies and daily energy intake in subjects with nonT2D, prediabetes, and T2D. Left panel: shows individuals' self-reported number of meals per day preceding the study center visit ranging from 1 to 6, number of subjects (N) assigned to the mean-number are shown in brackets below the meal number in gray. Individuals are grouped according to diabetes status (left column) and the number of individuals per group (N) are shown in gray. Sizes of the blue circles are referring to the proportion of subjects within each group. Panel in the middle: shows the type of meal noted above. The size of the blue circles indicates the number of individuals within each group (same as in the left panel) reported to have had the indicated type of meal. Right panel: boxplot showing the long-term usual calorie intake in kcal per day for each group (as indicated in the left panel, color code as in A). In total, 7.1% of nonT2D, 10.1% of prediabetes, and 20.2% of T2D no or insufficient information

(B) Boxplots illustrated the general intake of macro nutrients: energy intake [kcal/d] (nonT2D = 1114.50 ± 1304.70; prediabetes = 1110.74 ± 1337.69; T2D = 914.21 ± 1386.65; p value = 0.72), fiber [mg/d] (nonT2D = 13031.18 ± 9421.08; prediabetes = 12606.54 ± 9529.90; T2D = 11366.77 ± 9455.23; p value = 0.76), water-insoluble fiber [mg/d] (nonT2D = 8654.83 ± 6475.80; prediabetes = 8325.33 ± 6516.57; T2D = 7488.11 ± 6487.03; p value = 0.77) and water-soluble fiber [mg/d] (nonT2D = 4048.09 ± 3310.40; prediabetes = 3911.26 ± 3330.361; T2D = 3464.94 ± 3346.22; p value = 0.775), stratified according to the diabetes status. Color code as indicated.

UK (TwinsUK; N = 1,399 including N = 1,259 nonT2D, N = 46 iT2D, and N = 94 pT2D cases) performed substantially worse in classifying T2D (AUC = 0.68 for pT2D) and predicting incident T2D (AUC = 0.69 for iT2D) (Figures S3C–S3E; Table S8). This concords with previously published data from a Chinese study with cohorts from different districts (He et al., 2018).

We next addressed the question of whether these 13 s-arOTUs are also able to predict T2D in the prospective arm of KORA, which included 699 paired samples from 2013 and 2018 with 17 persisting T2D (pT2D) and 20 newly incident T2D (iT2D) cases (Figure 6A; Table S4). Here, rhythmicity was found for *alpha*-diversity, phyla proportions, and taxa in nonT2D but were lost for T2D cases (Figures 6B and S3A). Similar to the cross-sectional analysis (Figure 5C), the GLM was able to predict individuals at risk of developing T2D with an AUC of 0.69 (s-arOTUs) and 0.78 (s-arOTUs + BMI) (Figures 6C and S3C).

Functional Analysis of Rhythmic Microbiota and Their Association with T2D

We finally investigated functional changes within the fecal microbiome across diabetes disease states in the predictive subcohort of KORA by performing shotgun metagenomic in paired samples (from 2013 and 2018) from 50 KORA subjects (N = 100) (Figures 6D–6F). Subjects were selected based on an equal distribution of iT2D, nonT2D controls, and pT2D cases (Table S5). Functional pathways were identified using the HMP tool HUMAnN2 and annotated using KEGG. To identify those associated with diabetes, we applied a RF-based approach revealing an optimal set of 30 microbiome-encoded pathways (Figure S3F).

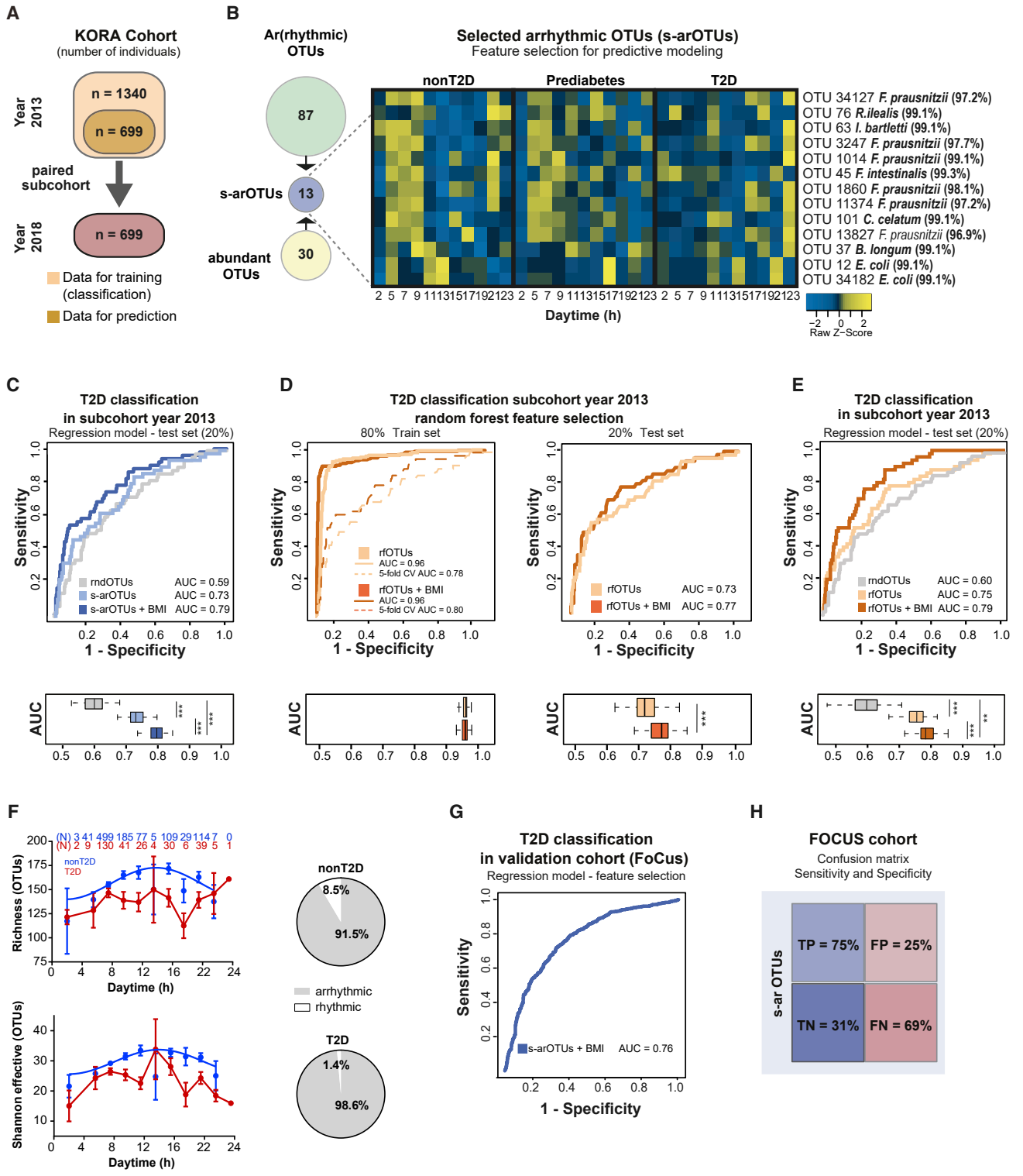

Figure 5. Arrhythmic Microbial Signature for Classification of T2D

(A) Number of KORA subjects of the prospective subcohort with samples from both years, 2013 and 2018 (N = 699; Table S4).

(B) Left panel: among the 87 arOTUs (green circle), which oscillated in controls (Figure 2G) but are arrhythmic in subjects with T2D or BMI ≥ 30, 13 OTUs (blue circle) showed differential rhythmicity based on DODR analysis and overlapped with the previously defined 30 OTUs (yellow circle) showing a significantly different relative abundance between nonT2D and T2D (Figure S1B). These 13 selected arrhythmic OTUs (s-arOTUs) were used for a further GLM (Table S7). Right panel: heatmap representing the relative abundance of the s-arOTUs according to the time-of-day different groups (e.g., nonT2D, prediabetes, and T2D). OTUs

(legend continued on next page)

Models created by including only these 30 top pathways distinguished between T2D and controls with a mean AUC of 0.81, while excluding them resulted in a significant reduction of AUC to 0.60 ($p < 8 \times 10^{-10}$, Mann-Whitney tests) (Table S6). In order to address the compositionality of microbial data, we repeated the above steps using centered log-scale transformed data (Tsilimigras and Fodor, 2016). The result remained unchanged with 27 of the 30 pathways retained and with similar patterns of AUC values (Figure S3G). This is indicative of a strong association between these pathways and T2D, including the metabolism of amino acids (phenylalanine, cysteine, methionine, alanine, glutamine, and aspartate), aromatic compounds (toluene, fluorobenzoate, and chlorocyclohexane), and fatty acids (alpha-linoleic acid and riboflavin) (Figures 6E, 6F, and S3H).

Twenty-six of the 30 pathways outlined above were associated (Spearman Correlation; false discovery rate (FDR) $\leq$ 0.1) with at least 2 of the 13 previously identified predictive s-arOTUs (Figure 6D; Table S6). The pathways could be partitioned into two different groups based on their association patterns with the s-arOTUs. While one group of pathways (G1) was associated with bacteria related to *E. coli* (i.e., those that had significant positive associations with clinical markers of T2D, such as fasting blood glucose, HOMA, and Hb1AC), the other (G2) showed associations with relatives of *F. prausnitzii* (negatively correlated with clinical markers of T2D) (Figure 6D). Strong positive correlations were observed between *E. coli* and xenobiotic metabolism, which are also negatively associated with short-chain fatty acid biosynthesis as well as metabolism of co-factors and vitamins. The *E. coli* group of taxa was negatively associated with the *F. prausnitzii* group, which mostly occurred in combination with *C. barletti* (Figure 6E). In contrast, *B. longum* was not associated with the presence of other taxa but negatively correlated with xenobiotic biodegradation pathways. We next determined whether the functional associations identified could be validated in datasets from previous studies. Previous major shotgun sequence data-based studies have investigated the gut microbiome alterations associated with T2D (Karlsson et al., 2013a, 2013b; Qin et al., 2012). While Karlsson et al. (2013a, 2013b) had primarily focused on elderly women above the age of 70 years, the cohort of Qin et al. (2012) had included individuals across a much wider age range (similar to the KORA cohort). Given this scenario, we compared differentially abundant genes from the study by Qin et al. (Qin et al., 2012) with the relative representation of the corresponding pathways in the T2D and nonT2D individuals of the KORA cohort (identified as either enriched in T2D or nonT2D). Notably, 19 of the 26 pathways could be validated in the Qin et al. cohort, along with their directionality (Figure 6D). The second unique characteristic of these functional markers was their association with the arrhythmic OTUs. Therefore, we next checked if any of these identified pathways were previously observed to show arrhythmic behaviors (or diurnal cycles). A recent study by Beli et al. (Beli et al., 2019) investigated the microbiome changes in the diurnal cycles of experimental murine T2D and control mice using a combination of metabolomics and predictive functional profiling of amplicon sequence data. Notably, seven of the 26 pathways identified here, including xenobiotic metabolism, cysteine and methionine metabolism, alpha-linoleic metabolism, and taurine and hypertaurine metabolism, were also reported to undergo diurnal rhythmicity in the study by Beli et al. (Figure 6D). Thus, the metagenomic analysis linked functions of the arrhythmic risk signature (s-arOTU) to the metabolic features of T2D (Figures 6E and 6F).

DISCUSSION

Extending a seminal study introducing the concept of rhythmicity of the gut microbiota in two individuals (Thaiss et al., 2014), here, we demonstrate diurnal oscillation of microbial taxa in three independent large-scaled populations (KORA, enable, and FoCus) and, using serial sampling, we even provide evidence for circadian rhythmicity of the microbiota profiles in one healthy subject. In addition, we demonstrate that T2D is associated with a disruption of gut microbiota rhythmicity and most importantly, we identified a risk pattern of arrhythmic taxa, which significantly contributes to the classification of T2D. A hypothesis-free machine-learning strategy confirmed the predictive validity of the selected arrhythmic OTUs. Disrupted microbial oscillation and the validity of this model to discriminate T2D from healthy populations were validated in the KORA-independent FoCus cohort. Interestingly, we also detected disrupted rhythmicity in the microbiota of obese individuals, but there was little overlap between arrhythmic OTUs of obese and diabetic individuals, indicating that BMI contributes to T2D risk stratification independent of disrupted circadian rhythms in the microbiome. In addition to BMI, we used several

given on the right are shown with their proposed species name (rRNA fragment identity given in brackets; bold indicates identity values to known species $\geq$ 97%) (proxy for species level).

(C) Curves of receiver operating characteristics (ROC) for classification of T2D in an independent test set. The GLM is based on 13 s-arOTUs (dark blue), 13s-arOTUS + BMI (light blue) as well as on 100 times randomly selected sets of each 13 OTUs (gray curve). The distribution of AUCs are shown by boxplots and are significantly different between the model types.

(D) ROC curve for a RF model using a training set (train set) of 80% of the data (dashed lines in the left panel) as well as using a test set with the remaining 20% of the data (ROC curves in the right panel). The mean AUC over 100 random data splits is shown. The boxplots below show the distribution of AUCs across all generated models for the corresponding training and test sets, respectively.

(E) ROC curve for classification of T2D in an independent test set consisting of 20% of the data. The GLM is based on 14 selected OTUs (rfOTUs; light orange), 14 rfOTUs + BMI (dark orange) as well as on the average performance of 100 random sets of each 14 OTUs (rndOTUs, gray curve). The distribution of AUCs of all models is shown by boxplots and differed significantly between the three model types.

(F) Circadian analysis of the FoCus cohort. Left panel: diurnal profiles of *alpha*-diversity in 1,363 subjects. Significant rhythms are illustrated with fitted cosine-wave curves (cosine-wave regression, $p \leq 0.05$, non-significance is shown by straight lines between data points. Right panel: amount of rhythmic (white) and arrhythmic (gray) OTUs and their relative abundance in percent. Data are represented as mean ± SEM.

(G) ROC curve for classification of T2D in the FoCus cohort. The curve was calculated by the imported GLM generated in KORA using the relative abundance values from the 13 assigned OTUs in the FoCus cohort + BMI (as in Figure 3H).

(H) Confusion matrix for the classification of T2D in the FoCus cohort. Shows the true positive (sensitivity) and true negative values (blue) as well as the false positive and false negative (specificity) values.

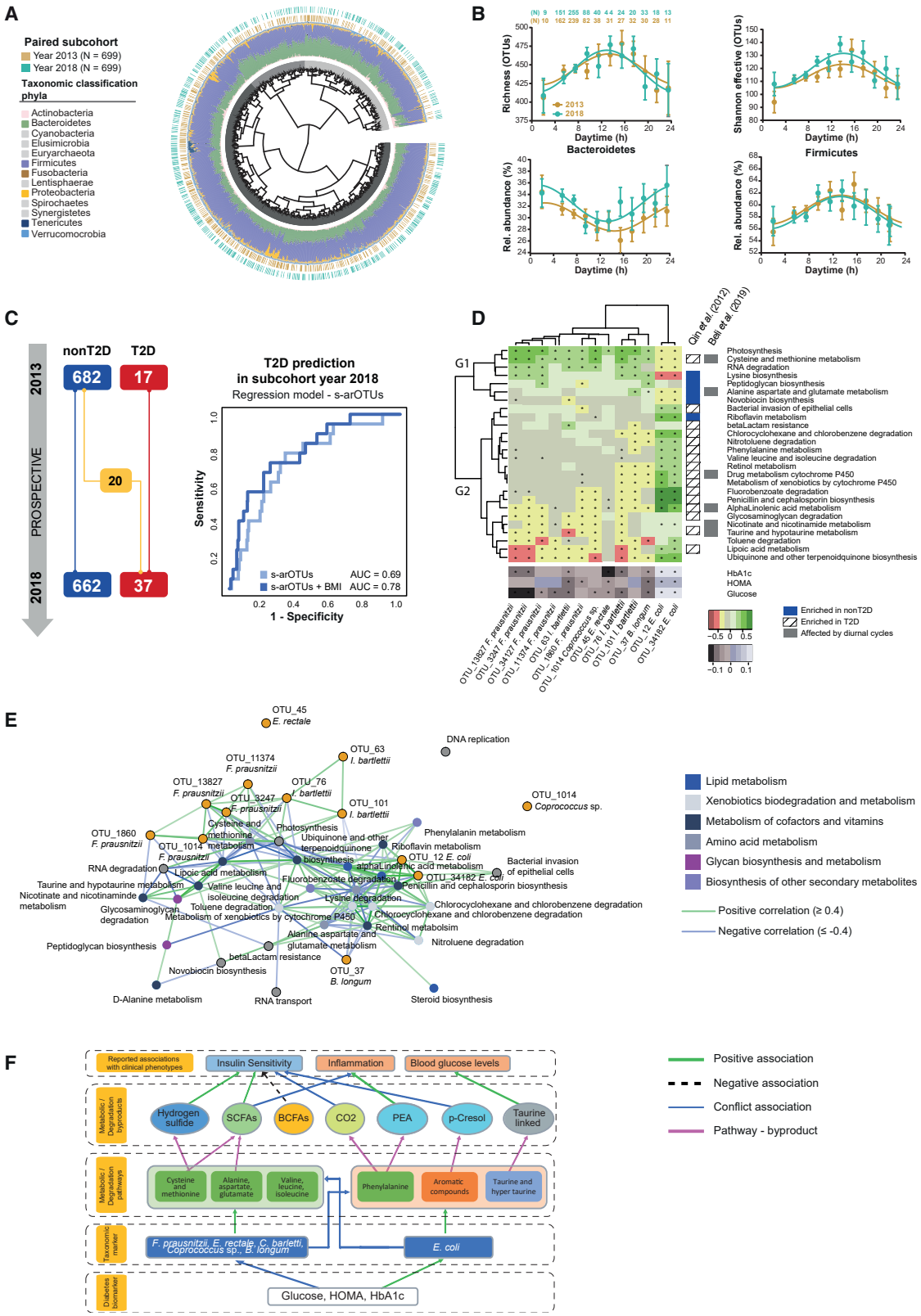

Figure 6. Arrhythmic Microbial Signature for Prediction of T2D and T2D-Associated Functional Pathways

(A) Phylogenetic tree of 1,401 paired individuals from year 2013 and year 2018 (similarly composed as Figure 1E). Subjects are grouped according to their similarity in their microbial profile calculated by generalized UniFrac distance. Based on unsupervised hierarchical clustering, individuals are assigned into three

(legend continued on next page)

other markers related to metabolic syndrome and insulin resistance to improve T2D classification, but in all combinations, the 13 selected arrhythmic bacterial taxa significantly contributed to the risk profiling of T2D. Although arrhythmic bacterial signatures have an additional value for the classification of T2D, these results aim at not replacing commonly used diabetes risk markers but rather support the hypothesis that daily oscillations of microbial profiles are functionally linked to metabolic health. Considering the loss of predictive validity of our model in the TwinsUK cohort, we cannot exclude the possibility that regional differences in individual microbiota profiles affect the repertoire of selected arrhythmic bacteria in T2D, emphasizing the need to acquire the daily time points of stool sampling for better interpretations of population data. In addition to regional differences (He et al., 2018), another possible limitation for the applicability of T2D risk signatures are the different diabetes classifiers. In the prospective part of the KORA cohort from year 2018, T2D was classified based on HbA1c, whereas TwinsUK used fasting blood glucose and FoCus the HOMA index. Even though all these measurements are based on values measured in blood and represent accepted biomarkers, some of the T2D cases might be misclassified by either one. Differences in the reported arrhythmic taxa between our study and the report from Thaiss et al. may again be explained by variations in microbiota composition of the different subjects at the individual and regional level, but also methodological differences in the study design, such as differences in the 16S rRNA variable target gene region for amplicon sequencing (KORA, FoCus, and enable: V3/V4, TwinUK: V4, Thaiss et al.: V1/2) and the sampling intervals (2 versus 6 h) allowing a better resolution in this study.

The development of obesity and T2D has been associated with circadian clock disruption (e.g., shift work) and gut microbiota dysbiosis (Marcheva et al., 2010; Pedersen et al., 2016; Qin et al., 2012; Szosland, 2010; Zhou et al., 2019). Despite emerging evidence for an interrelated dependency of microbiota and the host circadian system, we cannot completely exclude shift work schedules in T2D, eating behavior, or the microbial communities themselves as being driver(s) of oscillating bacterial population levels in the gut. Nevertheless, the patterns of daily food intake, mealtime, or number of meals per day showed no difference between healthy and diabetic individuals in KORA, suggesting that the observed arrhythmicity in fecal microbiota composition was independent of dietary habits. The circadian clock seems to be required to maintain rhythmicity of microbiota composition because oscillations are absent in mice with a genetically dysfunctional circadian clock (Liang et al., 2015; Thaiss et al., 2014). In addition, circadian signals from the microbiome affect diurnal rhythmicity of histone acetylation in intestinal epithelial cells controlling metabolic responses in the host (Kuang et al., 2019). This supports the hypothesis that circadian mechanisms of microbiota-host interactions contribute to metabolic homeostasis. Accordingly, loss of rhythmicity of taxa in T2D subjects identified in this study likely results in arrhythmicity of their metabolic products. Shotgun metagenomic analysis identified 26 microbial pathways associated with "xenobiotic," "branched-chain amino acids," "fatty acids" as well as "taurine metabolism," supporting a functional link between the diurnal oscillation of bacteria in the gut and metabolic homeostasis. Branched-chain amino acids were previously documented to follow circadian rhythmicity in blood samples from humans kept under 40-h constant routine, and their rhythmicity is lost in subjects with T2D (Skene et al., 2018). However, 19 of the 26 pathways (73%) identified by metagenomic analysis could be validated in a regionally independent cohort of T2D individuals (Qin et al., 2010), suggesting that the functionalities of arrhythmic microbiota are relevant biomarkers. Notable among these were pathways linked to the metabolism of certain amino acids and degradation of aromatic compounds. Among the amino acids, metabolism of alanine, aspartate, glutamate, and cysteine were positively associated with health (i.e., positive association with the health-associated taxonomic markers). The major (by-)products of the microbial fermentation of alanine, aspartate, glutamate, and cysteine are short-chain fatty acids (SCFAs) and hydrogen sulfide (H_2S), respectively (Oliphant and Allen-Vercoe, 2019). While the SCFAs are known for their health benefits including amelioration of insulin resistance, especially H_2S has been suggested as a positive regulator of insulin sensitivity (Khan et al., 2014). In contrast, the negative association with metabolic health observed for "phenylalanine

cluster C1 (N = 330), C2 (N = 918), and C3 (N = 167, colored in gray). Taxonomic composition on phyla level for each subject is shown as colored stacked barplots around the circle. Color bars around the circle are referring to the sample collection year (2013, brown; 2018, blue-green).

(B) Diurnal profiles of the relative abundance in *alpha*-diversity and the phyla of subjects from the KORA subcohort 2013 (N = 699, brown) or subcohort 2018 (N = 699, blue-green). Significant rhythms are illustrated with fitted cosine-wave curves (cosine-wave regression, $p \leq 0.05$). Data are represented as mean ± SEM.

(C) Predictive analysis of T2D in the paired KORA subcohort (samples from 2013, top and 2018, bottom). The prediction of incident T2D cases (iT2D) is based on the 13 s-arOTUs ± BMI in the regression model to the right. Baseline data is from nonT2D individuals from 2013. Endpoint is iT2D in 2018 (N = 20).

(D) The heatmap shows the Spearman correlations for 26 disease-predictive microbial pathways within the 13 OTUs becoming arrhythmic in T2D (across the 100 shotgun-sequenced metagenomes from 50 individuals, sampled 2013 and 2018). Only pathways that were significantly correlated with at least one of the 13 arrhythmic OTUs are shown. The heatmap on the bottom left shows the association pattern for the 13 OTUs with clinical markers characterizing T2D (across the entire cohort). Significant associations of both heatmaps were corrected using the Benjamini-Hochberg procedure. Corrected p values, which are ≤ 0.1 are indicated with × in each field. On the right, a one-dimensional heat-plot shows relative representations of each of the previous pathways observed in the cohort of Qin et al. (2012), either enriched in T2D (dashed) or enriched in nonT2D (blue). Furthermore, pathways predicted to be influenced by diurnal cycles in Beli et al. (2019) are indicated in brown if affected.

(E) Correlation network of HbA1c associated pathways in relation to selected T2D markers (s-arOTUs; orange circles). Green and blue lines indicate positive and negative associations, respectively. The thickness of lines is proportional to correlation coefficients. The color of circles indicating metabolites refers to functional classes as indicated.

(F) A schematic flow, integrating T2D signature, rhythmicity, and microbiome function of the metagenome data. The flow correlates the major disease-associated metabolic pathways identified in this study, their associations with the disease/health-associated taxonomic markers, the metabolic (by-)products originating from these pathways, and the previously known associations of these (by-)products with the various clinical phenotypes. The green and dashed black arrows indicate positive and negative associations, respectively. Conflicting associations are visualized by blue arrows (BCFA has been shown to be positively associated to insulin sensitivity in some studies, whereas others showed no association). Purple arrows link pathways to their metabolic (by-)products.

metabolism" had been attributed to phenylethylamine and carbon dioxide (Khan et al., 2014; Oliphant and Allen-Vercoe, 2019). In a similar manner, p-cresol derived from the degradation of aromatic compounds, such as toluene is suggested to be a negative regulator of insulin sensitivity (Koppe et al., 2013).

Taken together, loss of diurnal oscillation in gut microbiota composition and associated rhythmic functions may contribute to the development of metabolic disorders. Whether disease-associated arrhythmic taxa and their functionality are causally linked to the metabolic phenotype of T2D remains to be studied, but these findings clearly highlight the need to consider diurnal changes in the gut microbiome for diagnostic and prognostic investigations.

STAR★METHODS

Detailed methods are provided in the online version of this paper and include the following:

- KEY RESOURCES TABLE
- RESOURCE AVAILABILITY
  - Lead Contact
  - Materials Availability
  - Data and Code Availability
- EXPERIMENTAL MODEL AND SUBJECT DETAILS
  - Longitudinal Large-Scale Population-Based Cohort
  - Prospective Sub Cohort within KORA
  - Validation Cohort – TwinsUK
  - Validation Cohort – Enable
  - Validation Cohort – FoCus
  - Longitudinal Individual Data
- METHOD DETAILS
  - High-Throughput 16S rRNA Gene Amplicon Sequencing
  - Amplicon Sequence Analysis
- QUANTIFICATION AND STATISTICAL ANALYSIS
  - Statistical Analysis
  - Prospective Data
  - Diurnal Analysis of Microbiome Data Sets
  - Illustration of Diurnal Profiles
  - Detection of Selected Arrhythmic OTUs
  - Classification Model
  - Prognostic Model for T2D
  - Metagenomic Data Selection

SUPPLEMENTAL INFORMATION

Supplemental Information can be found online at https://doi.org/10.1016/j.chom.2020.06.004.

ACKNOWLEDGMENTS

The KORA study was initiated and financed by the Helmholtz Zentrum München – German Research Center for Environmental Health, which is funded by the German Federal Ministry of Education and Research (BMBF) and by the State of Bavaria. TwinsUK is funded by the Wellcome Trust, Medical Research Council, European Union, Chronic Disease Research Foundation (CDRF), and the National Institute for Health Research (NIHR)-funded BioResource, Clinical Research Facility, and Biomedical Research Centre based at Guy's and St Thomas' NHS Foundation Trust in partnership with King's College London. The Technical University of Munich provided funding for the ZIEL Institute for Food & Health and technical assistance, Caroline Ziegler and Angela Sachsenhauser provided outstanding technical support for sample preparation and 16S rRNA gene amplicon sequencing.

D.H., J.B., and S.K. received funding by the German Research Foundation (DFG, Deutsche Forschungsgemeinschaft) SFB 1371 (no. 395357507). D.H., T.S., and H.H. were supported by the "enable" Cluster funded by a grant of the German Federal Ministry of Education and Research (BMBF) FK 01EA1409A. D.H., T.C., A.P., T.S., and P.W.O.T. received funding from European Union Joint Programming Initiative DINAMIC (no. 2815ERA04E), supported by national funding agencies as follows: Science Foundation Ireland (P.W.O.T.), German Federal Ministry of Education and Research (D.H. and T.C.). J.B. was financially supported by VILLUM Young Investigator grant no. 13154.

AUTHOR CONTRIBUTIONS

D.H. conceived and coordinated the project; S.R., S.K., and T.C. performed 16S rRNA gene sequencing data analysis; E.L.A. and T.S.G. performed shotgun metagenomics and data analysis; T.A.B. and J.L. provided dietary information for KORA; S.R. and M.L. performed bioinformatics analysis; D.H., T.C., P.O.T., and J.B. supervised the work and data analysis; K.N. supported sample preparation and 16S rRNA gene sequencing analysis; M.L. processed data from the FoCus cohort; B.B., T.S., and H.H. provided samples from the enable cohort; A.F. provided help for sample analysis; H.G., M.T., W.R., and A.P.; provided KORA data and performed sample collection. C.I.L.R., J.T.B., and T.S. provided TwinsUK data; D.H., T.C., A.P., T.S., and P.W.O.T. secured funding; S.R., S.K., T.C., M.L., T.S.G., P.O.T., and D.H. wrote the manuscript. All authors reviewed the manuscript.

DECLARATION OF INTERESTS

The authors declare no competing interests.

Received: February 23, 2020
Revised: May 8, 2020
Accepted: June 8, 2020
Published: July 2, 2020

REFERENCES

Altschul, S.F., Gish, W., Miller, W., Myers, E.W., and Lipman, D.J. (1990). Basic local alignment search tool. Journal of Molecular Biology *215* (3), 403–410.

Arumugam, M., Raes, J., Pelletier, E., Le Paslier, D., Yamada, T., Mende, D.R., Fernandes, G.R., Tap, J., Bruls, T., Batto, J.M., et al. (2011). Enterotypes of the human gut microbiome. Nature *473*, 174–180.

Babicki, S., Arndt, D., Marcu, A., Liang, Y., Grant, J.R., Maciejewski, A., and Wishart, D.S. (2016). Heatmapper: web-enabled heat mapping for all. Nucleic Acids Res. *44*, W147–W153.

Barnea, M., Haviv, L., Gutman, R., Chapnik, N., Madar, Z., and Froy, O. (2012). Metformin affects the circadian clock and metabolic rhythms in a tissue-specific manner. Biochim. Biophys. Acta *1822*, 1796–1806.

Beli, E., Prabakaran, S., Krishnan, P., Evans-Molina, C., and Grant, M.B. (2019). Loss of diurnal oscillatory rhythms in gut microbiota correlates with changes in circulating metabolites in type 2 diabetic db/db mice. Nutrients *11*, 2310.

Berry, D., Ben Mahfoudh, K., Wagner, M., and Loy, A. (2011). Barcoded primers used in multiplex amplicon pyrosequencing bias amplification. Appl. Environ. Microbiol. *77*, 7846–7849.

Biecek, P. (2018). DALEX: Explainers for Complex Predictive Models in R. Journal of Machine Learning Research *19* (84), 1–5.

Breiman, L. (2001). Machine Learning *45* (1), 5–32.

Collado, M.C., Engen, P.A., Bandín, C., Cabrera-Rubio, R., Voigt, R.M., Green, S.J., Naqib, A., Keshavarzian, A., Scheer, F.A.J.L., and Garaulet, M. (2018). Timing of food intake impacts daily rhythms of human salivary microbiota: a randomized, crossover study. FASEB J. *32*, 2060–2072.

Edgar, R.C. (2013). Uparse: highly accurate OTU sequences from microbial amplicon reads. Nat. Methods *10*, 996–998.

Edgar, R.C., Haas, B.J., Clemente, J.C., Quince, C., and Knight, R. (2011). UCHIME improves sensitivity and speed of chimera detection. Bioinformatics *27*, 2194–2200.

Falony, G., Joossens, M., Vieira-Silva, S., Wang, J., Darzi, Y., Faust, K., Kurilshikov, A., Bonder, M.J., Valles-Colomer, M., Vandeputte, D., et al. (2016). Population-level analysis of gut microbiome variation. Science *352*, 560–564.

Forslund, K., Hildebrand, F., Nielsen, T., Falony, G., Le Chatelier, E., Sunagawa, S., Prifti, E., Vieira-Silva, S., Gudmundsdottir, V., Pedersen, H.K., et al. (2015). Disentangling type 2 diabetes and metformin treatment signatures in the human gut microbiota. Nature *528*, 262–266.

Franzosa, E.A., McIver, L.J., Rahnavard, G., Thompson, L.R., Schirmer, M., Weingart, G., Lipson, K.S., Knight, R., Caporaso, J.G., Segata, N., and Huttenhower, C. (2018). Species-level functional profiling of metagenomes and metatranscriptomes. Nat. Methods *15*, 962–968.

Godon, J.J., Zumstein, E., Dabert, P., Habouzit, F., and Moletta, R. (1997). Molecular microbial diversity of an anaerobic digestor as determined by small-subunit rDNA sequence analysis. Appl. Environ. Microbiol. *63*, 2802–2813.

Goodrich, J.K., Waters, J.L., Poole, A.C., Sutter, J.L., Koren, O., Blekhman, R., Beaumont, M., Van Treuren, W., Knight, R., Bell, J.T., et al. (2014). Human genetics shape the gut microbiome. Cell *159*, 789–799.

He, Y., Wu, W., Zheng, H.M., Li, P., McDonald, D., Sheng, H.-F., Chen, M.-X., Chen, Z.-H., Ji, G.-Y., Zheng, Z.-D.-X., et al. (2018). Regional variation limits applications of healthy gut microbiome reference ranges and disease models. Nat. Med. *24*, 1532–1535.

He, Z., Zhang, H., Gao, S., Lercher, M.J., Chen, W.H., and Hu, S. (2016). Evolview v2: an online visualization and management tool for customized and annotated phylogenetic trees. Nucleic Acids Res *44*, W236–241.

Holle, R., Happich, M., Löwel, H., and Wichmann, H.E.; MONICA/KORA Study Group (2005). KORA–a research platform for population based health research. Gesundheitswesen *67*, S19–S25.

Hughes, M.E., DiTacchio, L., Hayes, K.R., Vollmers, C., Pulivarthy, S., Baggs, J.E., Panda, S., and Hogenesch, J.B. (2009). Harmonics of circadian gene transcription in mammals. PLoS Genet. *5*, e1000442.

Hughes, M.E., Hogenesch, J.B., and Kornacker, K. (2010). JTK_CYCLE: an efficient nonparametric algorithm for detecting rhythmic components in genome-scale data sets. J. Biol. Rhythms *25*, 372–380.

Kaczmarek, J.L., Musaad, S.M., and Holscher, H.D. (2017). Time of day and eating behaviors are associated with the composition and function of the human gastrointestinal microbiota. Am. J. Clin. Nutr. *106*, 1220–1231.

Kanehisa, M., and Goto, S. (2000). KEGG: Kyoto encyclopedia of genes and genomes. Nucleic Acids Res. *28*, 27–30.

Karlsson, F., Tremaroli, V., Nielsen, J., and Bäckhed, F. (2013a). Assessing the human gut microbiota in metabolic diseases. Diabetes *62*, 3341–3349.

Karlsson, F.H., Tremaroli, V., Nookaew, I., Bergström, G., Behre, C.J., Fagerberg, B., Nielsen, J., and Bäckhed, F. (2013b). Gut metagenome in European women with normal, impaired and diabetic glucose control. Nature *498*, 99–103.

Khan, M.T., Nieuwdorp, M., and Bäckhed, F. (2014). Microbial modulation of insulin sensitivity. Cell Metab. *20*, 753–760.

King, B.M., Ivester, A.N., Burgess, P.D., Shappell, K.M., Coleman, K.L., Cespedes, V.M., Pruitt, H.S., Burden, G.K., and Bour, E.S. (2016). Adults with obesity underreport high-calorie foods in the home. Health Behav. Policy Rev. *3*, 439–443.

Koppe, L., Pillon, N.J., Vella, R.E., Croze, M.L., Pelletier, C.C., Chambert, S., Massy, Z., Glorieux, G., Vanholder, R., Dugenet, Y., et al. (2013). p-cresyl sulfate promotes insulin resistance associated with CKD. J. Am. Soc. Nephrol. *24*, 88–99.

Kozich, J.J., Westcott, S.L., Baxter, N.T., Highlander, S.K., and Schloss, P.D. (2013). Development of a dual-index sequencing strategy and curation pipeline for analyzing amplicon sequence data on the MiSeq Illumina sequencing platform. Appl. Environ. Microbiol. *79*, 5112–5120.

Kuang, Z., Wang, Y., Li, Y., Ye, C., Ruhn, K.A., Behrendt, C.L., Olson, E.N., and Hooper, L.V. (2019). The intestinal microbiota programs diurnal rhythms in host metabolism through histone deacetylase 3. Science *365*, 1428–1434.

Kumar, S., Stecher, G., Li, M., Knyaz, C., and Tamura, K. (2018). MEGA X: Molecular evolutionary genetics analysis across computing platforms. Mol. Biol. Evol. *35*, 1547–1549.

Lagkouvardos, I., Fischer, S., Kumar, N., and Clavel, T. (2017). Rhea: a transparent and modular R pipeline for microbial profiling based on 16S rRNA gene amplicons. PeerJ *5*, e2836.

Lagkouvardos, I., Joseph, D., Kapfhammer, M., Giritli, S., Horn, M., Haller, D., and Clavel, T. (2016). IMNGS: a comprehensive open resource of processed 16S rRNA microbial profiles for ecology and diversity studies. Sci. Rep. *6*, 33721.

Leone, V., Gibbons, S.M., Martinez, K., Hutchison, A.L., Huang, E.Y., Cham, C.M., Pierre, J.F., Heneghan, A.F., Nadimpalli, A., Hubert, N., et al. (2015). Effects of diurnal variation of gut microbes and high-fat feeding on host circadian clock function and metabolism. Cell Host Microbe *17*, 681–689.

Liang, X., Bushman, F.D., and FitzGerald, G.A. (2015). Rhythmicity of the intestinal microbiota is regulated by gender and the host circadian clock. Proc. Natl. Acad. Sci. USA *112*, 10479–10484.

Marcheva, B., Ramsey, K.M., Buhr, E.D., Kobayashi, Y., Su, H., Ko, C.H., Ivanova, G., Omura, C., Mo, S., Vitaterna, M.H., et al. (2010). Disruption of the clock components CLOCK and BMAL1 leads to hypoinsulinaemia and diabetes. Nature *466*, 627–631.

Oksanen, A., Blanchet, F.G., Friendly, M., Kindt, R., Legendre, P., McGlinn, D., Minchin, P.R., O'Hara, R.B., Simpson, G.L., Solymos, P., et al. (2019). vegan: Community Ecology Package. R package version 2.5-6.

Oliphant, K., and Allen-Vercoe, E. (2019). Macronutrient metabolism by the human gut microbiome: major fermentation by-products and their impact on host health. Microbiome *7*, 91.

Onaolapo, A.Y., and Onaolapo, O.J. (2018). Circadian dysrhythmia-linked diabetes mellitus: examining melatonin's roles in prophylaxis and management. World J. Diabetes *9*, 99–114.

Panda, S. (2019). The arrival of circadian medicine. Nat. Rev. Endocrinol. *15*, 67–69.

Pascal, V., Pozuelo, M., Borruel, N., Casellas, F., Campos, D., Santiago, A., Martinez, X., Varela, E., Sarrabayrouse, G., Machiels, K., et al. (2017). A microbial signature for Crohn's disease. Gut *66*, 813–822.

Pedersen, H.K., Gudmundsdottir, V., Nielsen, H.B., Hyotylainen, T., Nielsen, T., Jensen, B.A., Forslund, K., Hildebrand, F., Prifti, E., Falony, G., et al. (2016). Human gut microbes impact host serum metabolome and insulin sensitivity. Nature *535*, 376–381.

Pryor, R., Norvaisas, P., Marinos, G., Best, L., Thingholm, L.B., Quintaneiro, L.M., De Haes, W., Esser, D., Waschina, S., Lujan, C., et al. (2019). Host-microbe-drug-nutrient screen identifies bacterial effectors of Metformin therapy. Cell *178*, 1299–1312.e29.

Qin, J., Li, Y., Cai, Z., Li, S., Zhu, J., Zhang, F., Liang, S., Zhang, W., Guan, Y., Shen, D., et al. (2012). A metagenome-wide association study of gut microbiota in type 2 diabetes. Nature *490*, 55–60.

Qin, J., Li, R., Raes, J., Arumugam, M., Burgdorf, K.S., Manichanh, C., Nielsen, T., Pons, N., Levenez, F., Yamada, T., et al. (2010). A human gut microbial gene catalogue established by metagenomic sequencing. Nature *464*, 59–65.

Quast, C., Pruesse, E., Yilmaz, P., Gerken, J., Schweer, T., Yarza, P., Peplies, J., and Glöckner, F.O. (2013). The SILVA ribosomal RNA gene database project: improved data processing and web-based tools. Nucleic Acids Res. *41*, D590–D596.

Reitmeier, S., Hitch, T.C.A., Fikas, N., Hausmann, B., Ramer-Tait, A.E., Neuhaus, K., Berry, D., Haller, D., Lagkouvardos, I., and Clavel, T. (2020). Handling of spurious sequences affects the outcome of high-throughput 16S rRNA gene amplicon profiling. Research Square https://www.researchsquare.com/article/rs-11835/v1.

Relling, I., Akcay, G., Fangmann, D., Knappe, C., Schulte, D.M., Hartmann, K., Müller, N., Türk, K., Dempfle, A., Franke, A., et al. (2018). Role of wnt5a in metabolic inflammation in humans. J. Clin. Endocrinol. Metab. *103*, 4253–4264.

Revelle, W. (2019). psych: Procedures for Psychological, Psychometric, and Personality Research. Northwestern University, Evanston, Illinois. R package version 1.9.12.

Segata, N., Börnigen, D., Morgan, X.C., and Huttenhower, C. (2013). PhyloPhlAn is a new method for improved phylogenetic and taxonomic placement of microbes. Nat. Commun. *4*, 2304.

Segata, N., Waldron, L., Ballarini, A., Narasimhan, V., Jousson, O., and Huttenhower, C. (2012). Metagenomic microbial community profiling using unique clade-specific marker genes. Nat. Methods *9*, 811–814.

Skene, D.J., Skornyakov, E., Chowdhury, N.R., Gajula, R.P., Middleton, B., Satterfield, B.C., Porter, K.I., Van Dongen, H.P.A., and Gaddameedhi, S. (2018). Separation of circadian- and behavior-driven metabolite rhythms in humans provides a window on peripheral oscillators and metabolism. Proc. Natl. Acad. Sci. USA *115*, 7825–7830.

Sonnenburg, J.L., and Bäckhed, F. (2016). Diet-microbiota interactions as moderators of human metabolism. Nature *535*, 56–64.

Stern, S.E., Williams, K., Ferrannini, E., DeFronzo, R.A., Bogardus, C., and Stern, M.P. (2005). Identification of individuals with insulin resistance using routine clinical measurements. Diabetes *54*, 333–339.

Szosland, D. (2010). Shift work and metabolic syndrome, diabetes mellitus and ischaemic heart disease. Int. J. Occup. Med. Environ. Health *23*, 287–291.

Thaben, P.F., and Westermark, P.O. (2016). Differential rhythmicity: detecting altered rhythmicity in biological data. Bioinformatics *32*, 2800–2808.

Thaiss, C.A., Zeevi, D., Levy, M., Zilberman-Schapira, G., Suez, J., Tengeler, A.C., Abramson, L., Katz, M.N., Korem, T., Zmora, N., et al. (2014). Transkingdom control of microbiota diurnal oscillations promotes metabolic homeostasis. Cell *159*, 514–529.

Thingholm, L.B., Rühlemann, M.C., Koch, M., Fuqua, B., Laucke, G., Boehm, R., Bang, C., Franzosa, E.A., Hübenthal, M., Rahnavard, A., et al. (2019). Obese individuals with and without type 2 diabetes show different gut microbial functional capacity and composition. Cell Host Microbe *26*, 252–264.e10.

Tsilimigras, M.C., and Fodor, A.A. (2016). Compositional data analysis of the microbiome: fundamentals, tools, and challenges. Ann. Epidemiol. *26*, 330–335.

Turnbaugh, P.J., Ley, R.E., Mahowald, M.A., Magrini, V., Mardis, E.R., and Gordon, J.I. (2006). An obesity-associated gut microbiome with increased capacity for energy harvest. Nature *444*, 1027–1031.

Wang, J., Gamazon, E.R., Pierce, B.L., Stranger, B.E., Im, H.K., Gibbons, R.D., Cox, N.J., Nicolae, D.L., and Chen, L.S. (2016). Imputing Gene Expression in Uncollected Tissues Within and Beyond GTEx. American Journal of Human Genetics.

Yatsunenko, T., Rey, F.E., Manary, M.J., Trehan, I., Dominguez-Bello, M.G., Contreras, M., Magris, M., Hidalgo, G., Baldassano, R.N., Anokhin, A.P., et al. (2012). Human gut microbiome viewed across age and geography. Nature *486*, 222–227.

Yoon, S.H., Ha, S.M., Kwon, S., Lim, J., Kim, Y., Seo, H., and Chun, J. (2017). Introducing EzBioCloud: a taxonomically united database of 16S rRNA gene sequences and whole-genome assemblies. Int. J. Syst. Evol. Microbiol. *67*, 1613–1617.

Zarrinpar, A., Chaix, A., Yooseph, S., and Panda, S. (2014). Diet and feeding pattern affect the diurnal dynamics of the gut microbiome. Cell Metab. *20*, 1006–1017.

Zhernakova, A., Kurilshikov, A., Bonder, M.J., Tigchelaar, E.F., Schirmer, M., Vatanen, T., Mujagic, Z., Vila, A.V., Falony, G., Vieira-Silva, S., et al. (2016). Population-based metagenomics analysis reveals markers for gut microbiome composition and diversity. Science *352*, 565–569.

Zhou, W., Sailani, M.R., Contrepois, K., Zhou, Y., Ahadi, S., Leopold, S.R., Zhang, M.J., Rao, V., Avina, M., Mishra, T., et al. (2019). Longitudinal multi-omics of host-microbe dynamics in prediabetes. Nature *569*, 663–671.

STAR★METHODS

KEY RESOURCES TABLE

REAGENT or RESOURCE	SOURCE	IDENTIFIER
Critical Commercial Assays		
NucleoSpin gDNA columns	Machery-Nagel	Cat# 740230.250
Rapid v2 chemistry	Illumina	Cat# FC-402-4021
Sequence-Based Reagents		
DNA stabilization solution	Invitek	Cat# 1038111100
16S rRNA gene Illumina sequencing primers	Kozich et al., 2013	341F-ovh and 785r-ovh
Magnetic beads	Beckman Coulter	Cat# A63882; RRID: SCR_008940
Mock community	ZymoBIOMICS	Cat# D6300
Software and Algorithms		
Graphpad Prism v8.0.2	Graphpad Software	https://www.graphpad.com/scientific-software/prism/; RRID: SCR_002798
RStudio	RStudio	https://rstudio.com/products/rstudio; RRID: SCR_000432
BLAST	Altschul et al., 1990	https://blast.ncbi.nlm.nih.gov
IMNGS	Lagkouvardos et al., 2016	https://www.imngs.org/
EvolView	He et al., 2016	https://www.evolgenius.info/
EzBiocloud	Yoon et al., 2017	https://www.ezbiocloud.net/
KEGG	Kanehisa and Goto, 2000	https://www.genome.jp/kegg/; RRID: SCR_016974
Heatmapper	(Babicki et al., 2016)	http://www.heatmapper.ca; RRID: SCR_016974
GraPhlAn	(Segata et al., 2013)	https://github.com/biobakery/graphlan
Rhea	Lagkouvardos et al., 2017	https://github.com/Lagkouvardos/Rhea
JTK_CYCLE	(Hughes et al., 2010)	https://www.r-project.org/
HUMAnN2	Franzosa et al., 2018	https://github.com/biobakery/humann
Psych R package	Revelle, 2019	https://cran.r-project.org/web/packages/psych/index.html
randomForest R package	Breiman, 2001	https://cran.r-project.org/web/packages/randomForest/randomForest.pdf; RRID: SCR_015718
metaphlan2	Segata et al., 2012	https://github.com/biobakery/metaphlan
MixRF R-package	Wang et al., 2016	https://cran.r-project.org/web/packages/MixRF/index.html
DALAX R-package	Biecek, 2018	https://cran.r-project.org/web/packages/DALEX/index.html
DODR R packages	Thaben and Westermark, 2016	https://cran.r-project.org/web/packages/DODR/index.html
vegan R package	Oksanen et al., 2019	https://rdrr.io/cran/vegan/; RRID: SCR_011950
Biological sample		
Healthy age-matched male adult, stool samples (N = 58)	Technical University Munich, Chair of Nutrition and Immunology	N/A
Enable Cohort, healthy age-matched individuals (N = 94 subjects, N = 357 stool samples), mean age 53 years, equal distribution male/female	Technical University Munich, Chair of Nutrition and Immunology	N/A

(*Continued on next page*)

Continued

REAGENT or RESOURCE	SOURCE	IDENTIFIER
Deposited Data		
Sequence data, analyses, and resources related to the 16S rRNA gene sequencing of enable cohort	This paper	SRA: PRJNA635239
Sequence data, analyses, and resources related to the 16S rRNA gene sequencing of S1	This paper	SRA: PRJNA635239
Other		
Sequence data, analyses, and resources related to the 16S rRNA gene sequencing of KORA cohort	This paper; Holle et al., 2005	https://epi.helmholtz-muenchen.de/
Sequence data, analyses, and resources related to the 16S rRNA gene sequencing of FoCus cohort	Relling et al., 2018	https://portal.popgen.de
Sequence data, analyses, and resources related to the 16S rRNA gene sequencing of TwinsUK cohort	Goodrich et al., 2014	SRA: PRJEB13747

RESOURCE AVAILABILITY

Lead Contact

Further information and requests for resources and reagents should be directed to and will be fulfilled by the Lead Contact, Dirk Haller (dirk.haller@tum.de).

Materials Availability

This study did not generate new unique reagents.

Data and Code Availability

There are restrictions to the availability of 16S rRNA gene sequencing data due to the informed consent given by the cohort study participants which does not allow the deposit of data in public databases. KORA data are available upon request from KORA by means of a project agreement (https://epi.helmholtz-muenchen.de/). Data of the FoCuS cohort is available from the PopGen/P2N biobank upon request (https://portal.popgen.de).

The accession number for the TwinsUk study raw sequencing data reported in this paper was accessed via the European Nucleotide Archive (ENA: PRJEB13747).

The accession number for the raw sequencing data as well as demographical informationof the enable cohort and longitudinal data from S1 reported in this paper are available via Sequence Read Archive (SRA: PRJNA635239). Software used to analyze the data are either freely or commercially available. Source code data are available from the corresponding author on request.

EXPERIMENTAL MODEL AND SUBJECT DETAILS

Longitudinal Large-Scale Population-Based Cohort

Fecal samples were collected from participants of the longitudinal population-based cohort S4 KORA study (Cooperative Health Research in the Augsburg Region) in southern Germany, which started in 1999 and focuses on cardio-metabolic health, especially diabetes. KORA-FF4 samples were collected as follow-up of the cohort in 2013/2014 (for simplicity referred to year 2013 in the text) and KORA-Fit in 2018, respectively. Detailed study design and methods have been published previously (Holle et al., 2005). For the data analysis, 100 stool samples were excluded due to medication issues and gut-related diseases. T2D and prediabetes were defined by oral glucose tolerance test or physicians-confirmation and classified by WHO in 2013. Cases with Type 1 Diabetes were excluded.

The investigations were carried out in accordance with the Declaration of Helsinki, including written informed consent of all participants. All study methods were approved by the ethics committee of the Bavarian Chamber of Physicians, Munich (KORA-FF4 2013/14 EC No. 06068 and KORA-Fit 2018/19 EC No. 17040). For further information about KORA-subject details see Holle et al. (2005) or contact the corresponding author.

Prospective Sub Cohort within KORA

In 2013, fecal samples were collected from 2,076 individuals. Prospectively a subset of 800 individuals were sampled again in 2018. Participants received sampling kit with collection tubes filled with 5 ml stool stabilizer (Invitek DNA Stool Stabilizer, No. 1038111100), and to store the samples in their household refrigerator as short as possible. After delivery samples were finally stored at -80°C at the study centre in Augsburg and thawing and freezing was prevented. A comprehensive data set on social-demographical characteristics, risk factors profiles, diet and medical history was ascertained amongst others.

Validation Cohort – TwinsUK

The collection of fecal samples, DNA extraction, amplification of the V4 hypervariable region of the 16S rRNA gene (primers 515F and 806R), purification and pooling were performed as previously described (Goodrich et al., 2014). The pooled amplicons were sequenced using the Illumina MiSeq platform with 2×250bp paired-end sequencing. The raw sequencing data was accessed via the European Nucleotide Archive (ENA: PRJEB13747). The analysis was performed on N = 1,399 individuals, including N = 46 incident Type 2 Diabetes cases as well as N = 94 Type 2 Diabetes cases that were classified using a combination of self-reported questionnaires as well as longitudinal glucose measurements. For further information about subjects details see Goodrich et al. (2014) or contact the corresponding author.

Validation Cohort – Enable

The enable study included healthy volunteers from the region of Munich/Freising in the south of Germany at four defined phases of life. Fecal samples were collected at the first visit between 2016-2018. From a subset of this cohort (N = 113, N = 50 males and N = 63 females, mean age of 53 years) three additional samples were collected at the time of the second visit, after another 4 weeks and after 12 weeks. The sample preparation and MiSeq sequencing of the V3-V4 hypervariable regions was performed as described above. After chimera checking and samples with low read counts were excluded. For the analysis N = 93 subjects with multiple time points are considered. The raw sequencing data was accessed via the European Nucleotide Archive (ENA: PRJNA635239). All study methods were approved by the ethics committee of the Technical University of Munich, School of Medicine (enable No. 452/15S). Written informed consent was obtained from all subjects.

Validation Cohort – FoCus

The cohort originated from the Food Chain Plus (FoCus) project from 2011 to 2014. Sample collection and DNA preparation were performed by the IKMB in Kiel, Germany as described previously (Relling et al., 2018) 16S rRNA gene sequencing targeting the V3-V4 region was performed following the standard protocols as described above. In total 1,529 fecal samples were sequenced. Samples with low read counts were excluded as well as samples with missing information in BMI, HOMA index values and sampling time point. For the analysis 1,363 subjects are considered. T2D was classified based on HOMA index (T2D: HOMA > 5.0 (Stern et al., 2005)). For further information about subject details see Relling et al. (2018) or contact the corresponding author.

Longitudinal Individual Data

Consecutive fecal samples (n = 58) of a 50-year old male subject were collected over three years (starting July 2018 to February 2020). The subject S1 was classified as healthy age-matched subject based on medical records including the documentation for the absence of diseases such as T2D (and others) and the availability of annually recorded blood parameters demonstrating the metabolic health of S1 (BMI < 25, HbA1c in the normal range, blood glucose in the normal range, blood pressure in the normal range). Multiple timepoint sampling was conducted in four phases (July-August 2017 N = 22, December 2017 N = 12, February – March 2018 N = 15 and January 2020 N = 10). The sample preparation and MiSeq sequencing of the V3-V4 hypervariable regions was performed following the standard protocols as described above. For further information about subject details contact the corresponding author. The raw sequencing data was accessed via the European Nucleotide Archive (ENA: PRJNA635239). All study methods were approved by the ethics committee of the Technical University of Munich, School of Medicine (enable No. 452/15S). Written informed consent was obtained.

METHOD DETAILS

High-Throughput 16S rRNA Gene Amplicon Sequencing

Metagenomic DNA was isolated by a modified version of the protocol by Godon et al. (Godon et al., 1997) from 600-μl aliquots of stool mixed in DNA stabilization solution (Invitek). Briefly, microbial cells were lysed using a bead-beater with 0.1-mm glass beads (FastPrep-24 fitted with a cooling adapter). DNA was then purified on NucleoSpin gDNA columns (Machery-Nagel, No. 740230.250). DNA was either used immediately for amplicon analysis or kept frozen as aliquots of 35 μl for metagenomic analysis. After DNA extraction, all pipetting steps until sequencing were conducted using a robotized liquid handler to maximize reproducibility.

PCR were conducted in duplicates. DNA was diluted in PCR-grade water and used as template (24ng) for amplifying (25 cycles) the V3-V4 regions of 16S rRNA genes using primers 341F-ovh and 785r-ovh (Kozich et al., 2013) in a two-step process shown to minimize bias (Berry et al., 2011). PCR products were pooled during cleaning using magnetic beads (Beckman Coulter). PCR-fragment concentration was determined by fluorometry and adjusted to 2nM prior to pooling. The multiplexed samples were sequenced on an Illumina HiSeq in paired-end mode (2x250 bp) using the Rapid v2 chemistry. Analysis were based on chimera checked high-quality sequences, samples with low read counts were (< 4,700) were re-sequenced on an Illumina MiSeq using v3. Control sequencings have shown no difference between both machine types (data not shown). To control for artifacts and reproducibility between runs, two negative controls (a PCR control without template DNA and a DNA extraction control consisting of 600 μl Stool stabilizer without stool) as well as a positive control using a mock community (ZymoBIOMICS, No. D6300) were included throughout for every batch of 45 samples (processed on one single 96-well-plate).

Amplicon Sequence Analysis

Sequencing data was preprocessed using the IMNGS pipeline (Lagkouvardos et al., 2016). Five nucleotides on the 5' end and 3'end are trimmed for the R1 and R2 read, respectively (trim score 5) and an expected error rate of 1. Chimera were removed using UCHIME (Edgar et al., 2011) and the reads of de-multiplexed samples were merged and clustered by 97% similarity using UPARSE v8.1.1861_i86 (Edgar, 2013). OTUs occurring at a relative abundance < 0.25% across all samples were removed to prevent the analysis of spurious OTUs (Reitmeier et al., 2020). Taxonomy was assigned using the RDP classifier version 2.11 and confirmed using the SILVA database (Quast et al., 2013). For phylogenetic analyses, maximum-likelihood trees were generated by FastTree based on MUSCLE alignments in MegaX (Kumar et al., 2018). We used the EzBioCloud database (Yoon et al., 2017) for precise identification of OTU sequences of interest.

QUANTIFICATION AND STATISTICAL ANALYSIS

Statistical Analysis

Statistical analysis was performed in R version 3.5.0. Absolute read counts were normalized by minimum sum counts for the calculation of within samples diversity. The contribution of covariates towards differences in the microbial profile of the whole cohort was determined by using multivariate permutational analysis using the R function *adonis* from the *vegan package v.2.5-6*. The explained variation of a variable is shown in R^2 values and is considered as significant with a P-value $\leq$ 0.05. For the cumulative explained variation, all significant covariates are included in a multivariate model. Data was adjusted according to confounding factors (gender, age, BMI, physical activity, PPI, metformin, and vitamin D intake) as well as stratified according to phenotypical characteristics. Description of taxonomic composition is based on relative abundances. Between-sample diversity is calculated by generalized UniFrac using *GUniFrac* v1.1. distances. De-novo clustering is based on Ward hierarchical clustering, the selected number of clusters is chosen according to the Calinski and Harabasz index, performed with the R package *NbClust* v.3.0. For the analysis of prevalence of categorical variables between groups, a non-parametric Fisher test is used. Taxonomic differences between groups is determined by generalized linear model based on relative abundance adjusted for confounding. P-values were corrected for multiple testing using the Benjamini-Hochberg false discovery rate control procedure. Parts of this procedure have been assembled in the software pipeline Rhea (Lagkouvardos et al., 2017) used for this analysis.

Prospective Data

A subset of individuals from the KORA cross-sectional collection from 2013 was recruited again in 2018. Stool samples from 699 individuals were collected and paired-end sequenced on an Illumina MiSeq as described above. T2D was classified based on HbA1c value (%) an incident T2D case is defined as HbA1c < 6.5% in 2013 and HbA1c $\geq$ 6.5% in 2018 because oral glucose tolerance test was not available in 2018. Sequencing data from the sub-cohort of paired subjects is used to predict T2D. Subjects with unclassified T2D status are excluded. To avoid bias due to overfitting, the 699 samples from 2013, which are part of the 2018 follow-up dataset, are retained for independent validation.

Diurnal Analysis of Microbiome Data Sets

Statistical analyses were conducted with GraphPad Prism v6.01 (GraphPad Software) and the R script JTK_CYCLE v3.1.R (Hughes et al., 2010). To efficiently identify and characterize diurnal oscillations in large datasets, circadian variation was tested by fitting a cosine-wave equation: y = baseline+(amplitude$\cdot\cos(2\cdot\pi\cdot((x-[\text{phase shift})/24)))$ or a double harmonic cosine-wave equation: y = baseline+([amplitude A]$\cdot\cos(2\cdot\pi\cdot((x-[\text{phase shift A}])/24)))$ + ([amplitude B]$\cdot\cos(4\cdot\pi\cdot((x-[\text{phase shift B}])/24)))$ on *alpha*-diversity and relative abundance, with a fixed 24-h period. The goodness of fit was corrected for multiple comparisons and the significance was determined using an F-test. Results from the cosine- and harmonic cosine-wave regression were compared with a widely used rhythmicity detection algorithms JTK_CYCLE, which employs a non-parametric algorithm detecting sinusoidal signals (Hughes et al., 2010), whereby JTK presents the highest false negative rates (Hughes et al., 2009). Each pvalue was Bonferroni-adjusted for multiple testing. A statistically significant difference was assumed when p value $\leq$ 0.05. The high-density time sampling allowed the identification of diurnal-regulated microbiota with a high statistical power (Hughes et al., 2009).

Illustration of Diurnal Profiles

A high-resolution time course was generated by merging samples taken between 5:00 am and 24:00 pm in two-hour intervals, and a larger 4-hour interval at night from 00:01 am to 4:59 am to compensate for the low sample size in some groups during the night time points. The merged data points are illustrated using GraphPad Prism v6.01 (GraphPad Software) with the sample size of every groups per time point indicated below the data point +/-SEM in the individual graphs. To demonstrate the overall phase relationship and periodicity of all OTUs together, heatmaps have been generated using the online tool *Heatmapper* (http://www.heatmapper.ca; (Babicki et al., 2016). The raw data of each OTU were merged in the above indicated intervals, sorted by the peak phase based on cosine-wave regression analysis (described below) and scaled in each row according to the highest abundance of the OTU.

Detection of Selected Arrhythmic OTUs

The relative abundance of each OTU was assessed for a 24-hr rhythmicity using the cosine-wave regression. On total, 87 OTUs showed diurnal fluctuation in subjects with nonT2D, Prediabetes or a BMI < 30, whereas no significant rhythmicity was detected in subjects with T2D or BMI $\geq$ 30 for those OTUs (Figure 2F; Table S6). These 87 OTUs were further analyzed for differential 24-h time-of-day patterns using the Detection of Differential Rhythmicity (DODR) R packages (Thaben and Westermark, 2016). Resulting DODR P-values were corrected for multiple comparisons and at the corrected P $\leq$ 0.05 significance level DODR detected 26 OTUs, referring to as arOTUs, with significantly different 24-h time-of-day patterns when comparing nonT2D with T2D, prediabetes with T2D and BMI < 30 with BM $\geq$ 30 (Figure 2D). An overlap of these 26 arOTUs with the previously defined 30 OTUs (abundant OTUs), which showed a significantly different averaged abundance between nonT2D and T2D (Figure S1B, Table S7), identified 13 OTUs. The abundance of these 13 OTUs followed a 24-h rhythm in the control groups (nonT2D, BMI < 30), but were arrhythmic in T2D and BMI $\geq$ 30 and in addition significantly changed their abundance (s-arOTUs).

Classification Model

A machine-learning algorithm is applied to the cross-sectional data (N = 1,340) from 2013 to classify T2D, excluding the paired-sub-cohort (year 2013 N = 699; year 2018 N = 699). Further, the most prevalent (> 10%) and abundant (> 0.1%) OTUs are selected for the analysis, resulting in 425 OTUs. A random forest model was used to classify binary outcome variables based on a combination of BMI and microbial composition with a 5-fold cross validation by using *randomForest* from the R package *randomForest* v4.6-14. To receive a robust and generalizable classification model, the machine-learning algorithm was applied 100-times iteratively assigning individuals at random to either the training (80%) or test set (20%). For the training set, a subset of equally distributed T2D (N = 150) and nonT2D (N = 150) cases was taken to train the model (Figure S4D). The model was then validated on the 20% test set (Figures S4A and S4B). Based on out-of-bag error rates and Gini index, the most important features were selected for each iteration using *rfcv* from R package *randomForest* v4.6-14. Features which appeared in at least 50% of all 100 random forest models were considered as classification feature for the final model. Feature importance was also assessed via SHapley Additive exPlanations (SHAP) values using the R package DALAX v1.0.1 (Figure S4I). The training of a random forest model was repeated for centralized log ratio transformed as well as for log ratios of relative abundances (n = 70,000 pairs) to address compositionality of microbial data (Figure S4E). We further generated a mixed effect random forest model with BMI as random factor using the R package *MixRF* v1.0 and otherwise retaining the same procedure for selecting test and training data. The model selected 13 OTUs, two are overlapping with the selected arrhythmic OTUs (s-arOTUs) (Figures 3C and S4F).

Prognostic Model for T2D

For the risk prediction of T2D, a generalized linear model for binomial distribution and binary outcome (logit) was generated using the previously selected features based on arrhythmic OTUs including BMI as additional variable. For the model, a generalized linear model was generated on the cross-sectional cohort excluding the paired sub-cohort. To verify the importance of the selected features, a generalized linear model for control OTUs (rndOTUs, equal number of OTUs as in s-arOTUs) are implemented repetitively 100-times. The randomly selected control OTUs (rndOTUs) neither show rhythmicity in disease nor non-disease stages.

To apply the generated models to the unknown data from the paired sub-cohort of both time points, a blast search was performed assigning sequences of the selected features to the corresponding sequences of the new dataset. Sequences with an identify of 97%, coverage of 80% and an E value $\leq 10^{-5}$ are considered as a hit. If there is no matching sequence available when using the above thresholds, the best match is taken instead. Sequences are uniquely assigned to a reference sequence. For the prediction of T2D, the relative OTU abundance of year 2013 is considered as baseline. Individuals at this stage are not classified as T2D. The two endpoints are incident T2D cases and nonT2D in 2018. For the validation cohorts the corresponding OTUs were assigned by BLAST as well. Addressing the issue of different hypervariable region was possible since both cohorts overlap in the V4 region. Hence, the selection of s-arOTUs in the TwinsUK study was possible. To avoid any misclassification, we further checked the V4 sequences in EzBiocloud to guarantee the correct taxonomic assignment

Metagenomic Data Selection

From of the prospective data, we chose a subset of 100 paired individuals showing interesting phenotypic characteristics for shotgun sequencing and metabolomic analysis. The dataset includes incident T2D cases, T2D cases and nonT2D controls, which are otherwise metabolically healthy. Shotgun sequencing of the isolated DNA from stool samples, as well as the analysis, were conducted by the APC Microbiome Institute, Cork (Ireland).

The taxonomic and functional annotation of the shotgun feacal metagenomic datasets were performed using the *metaphlan2* (Segata et al., 2012) and HUMAnN2 (Franzosa et al., 2018) pipelines. Gene families detected using the HUMAnN2 approach were then mapped to the KEGG pathway orthology (Kanehisa and Goto, 2000) scheme using internal mappings within HUMAnN2. *Psych* R package v1.8.12 was used to compute the correlation between the OTU markers with the clinical markers and the KEGG pathways (Spearman correlation filtered with Benjamini-Hochberg corrected FDR $\leq$ 0.1). For identifying the top disease-predictive pathways, we used an iterative random forest approach *randomForest* from R package *randomForest* v4.6-14, where we performed 100 iterations, each time taking 50% of the samples with T2D (from both 2013 and 2018) and an equal number of controls and tested the

same model on the remaining 50%, again with an equal number of controls. Mean AUC and mean feature importance scores were then computed across iterations using standard R functions. For the validation in the cohort of Qin et al. (Qin et al., 2012) cohort, the pathway affiliations of the differentially abundant KEGG orthologues identified in this study were obtained. The relative representation of the marker pathways in the T2D-enriched and control-enriched were then computed. Pathways that were only detected in a group or had more than two-fold increase of representation in the given group were identified as enriched in that group (T2D or nonT2D), respectively.